

# Two Channel Filter Banks on Arbitrary Graphs with Positive Semi Definite Variation Operators

Eduardo Pavez, Benjamin Girault, Antonio Ortega, Philip A. Chou

**Abstract**—We propose novel two-channel filter banks for signals on graphs. Our designs can be applied to arbitrary graphs, given a positive semi definite variation operator, while using arbitrary vertex partitions for downsampling. The proposed generalized filter banks (GFBs) also satisfy several desirable properties including perfect reconstruction and critical sampling, while having efficient implementations. Our results generalize previous approaches that were only valid for the normalized Laplacian of bipartite graphs. Our approach is based on novel graph Fourier transforms (GFTs) given by the generalized eigenvectors of the variation operator. These GFTs are orthogonal in an alternative inner product space which depends on the downsampling and variation operators. Our key theoretical contribution is showing that the *spectral folding property* of the normalized Laplacian of bipartite graphs, at the core of bipartite filter bank theory, can be generalized for the proposed GFT if the inner product matrix is chosen properly. In addition, we study vertex domain and spectral domain properties of GFBs and illustrate their probabilistic interpretation using Gaussian graphical models. While GFBs can be defined given any choice of a vertex partition for downsampling, we propose an algorithm to optimize these partitions with a criterion that favors balanced partitions with large graph cuts, which are shown to lead to efficient and stable GFB implementations. Our numerical experiments show that partition-optimized GFBs can be implemented efficiently on 3D point clouds with hundreds of thousands of points (nodes), while also improving the color signal representation quality over competing state-of-the-art approaches.

**Index Terms**—two-channel filter banks, graph Fourier transform, graph signal, multiresolution representation

## I. INTRODUCTION

GRAPHS are powerful tools to model unstructured data. On a graph, nodes and edges represent objects of interest and their similarity relations, respectively. A function on the nodes is called a graph signal, with examples including color attributes in images and 3D point clouds, measurements obtained from sensor networks, or biomedical brain signals [1]. Graph signal processing (GSP) develops new theories and algorithms for restoration, compression, and analysis of graph signals [2]–[4]. Filter banks and other multiresolution representations (MRR) have been widely applied to signal processing problems on regular grids [5]–[8], which has motivated their generalization to graphs [2], [9].

*Bipartite Filter Banks* (BFBs) [10], [11] are critically sampled two-channel filter banks on bipartite graphs. They are

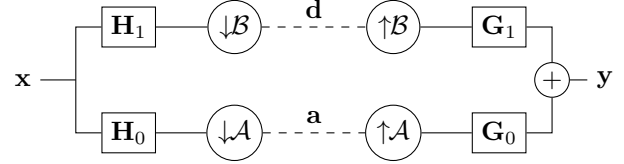


Fig. 1: Two-channel filter bank implemented with spectral graph filters. Low- and high-pass analysis filters are denoted by  $H_0$  and  $H_1$  respectively.  $G_0$  and  $G_1$  correspond to low- and high-pass synthesis filters.  $A$  and  $B$  are the sampling sets of the low- and high-pass channels respectively.  $x$  and  $y$  denote input and output signals respectively.  $a$  is the vector of approximation (low-pass) coefficients, and  $d$  is the vector of detail (high-pass) coefficients.

constructed with low- and high-pass spectral graph filters of the normalized graph Laplacian, along with downsampling and upsampling operators (see Figure 1). BFBs satisfy several desirable properties: (i) perfect reconstruction, (ii) critical sampling (non redundant), (iii) compact support (polynomial filters) and (iv) energy preservation (orthogonality). BFBs are closely related to filter bank designs for signals on regular grids since both satisfy the same design conditions, (i)–(iv), and specific design techniques (e.g., Meyer and Daubechies filters [5], [6]) can be adapted to construct BFBs [10]–[13]. Given their efficient implementations, close relation with filter banks on regular grids, and their well-understood theoretical properties, BFBs have found numerous applications in compression [14]–[17], denoising [18] and signal analysis [19]–[21]. However, a major limitation of BFBs is that they are only valid for bipartite graphs, using either the normalized Laplacian [10], [11] or the adjacency matrix [13], [22]. In practice, the graph in a given application is rarely bipartite, so that bipartite graph learning or bipartite approximation are required [23]–[27], which increases computational complexity significantly, and may hinder the signal representation quality. Another limitation of BFBs comes from their use of the normalized Laplacian (with lowest frequency eigenvector entries proportional to the node degree) instead of the combinatorial Laplacian (constant lowest frequency eigenvector entries), which is usually a better choice for signal representations and results in better energy compaction [11], [28], [29].

For discrete time signals, many filter bank designs obey properties (i)–(iv) [5], while others obeying (i)–(iii) are also used (e.g., near orthogonal separable filter banks [30]). These filter banks can be implemented efficiently by exploiting lifting structures, separable filtering and the *Fast Fourier Transform*

E. Pavez and A. Ortega are with the Department of Electrical and Computer Engineering, University of Southern California, Los Angeles, CA, USA. (e-mail: pavezcar@usc.edu, ortega@sipi.usc.edu). B. Girault is with Université de Rennes, ENSAI, CNRS, CREST-UMR 9194, Rennes, France. (e-mail: benjamin.girault@ensai.fr). P. A. Chou is with Google Research, Seattle, Washington, USA. (e-mail: philchou@google.com).

(FFT). In contrast, fast *Graph Fourier Transform* (GFT) algorithms are only available for very limited families of graphs [31], while separable and lifting structures are only known for bipartite graphs [10], [11], [22], thus preventing the use of these techniques for reduced complexity implementations on arbitrary graphs. We are motivated by 3D point cloud applications, where graphs can have millions of nodes [32] making it difficult to use higher complexity methods, e.g., filter banks that require eigendecomposition or bipartite graph learning. As a result, we seek designs that can leverage graph sparsity for efficient implementation, for instance by using low degree polynomial graph filters.

We generalize the critically sampled filter bank design problem so that solutions can be found for non-bipartite graphs, as well as with operators other than the normalized Laplacian. Instead, *Generalized Filter Bank* (GFB) solutions are obtained for *arbitrary graphs*, for *any positive semi-definite graph variation operator* and using *arbitrary vertex partitions for downsampling*, while still satisfying properties (i)–(iv). We show that for sparse graphs, GFBs have scalable and eigendecomposition-free implementations, relying only on sparse matrix-vector products and sparse linear system solvers.

The key innovation enabling GFBs is the adoption of a new inner product, which allows us to depart from the traditional Hilbert space (induced by the dot product) underlying the majority of GSP methods<sup>1</sup>. We build upon [29] where graphs are represented by a positive semi definite variation operator  $\mathbf{M} \succeq 0$ , which measures signal smoothness, and an inner product  $\langle \mathbf{x}, \mathbf{y} \rangle_{\mathbf{Q}} = \mathbf{y}^{\top} \mathbf{Q} \mathbf{x}$ , with  $\mathbf{Q} \succ 0$ . The  $(\mathbf{M}, \mathbf{Q})$  *Graph Fourier Transform* ( $(\mathbf{M}, \mathbf{Q})$ -GFT) is defined as the generalized eigenvectors of  $\mathbf{M}$ , which form a  $\mathbf{Q}$ -orthonormal basis.

In our solution,  $\mathbf{Q}$  is chosen as a function of  $\mathbf{M}$  and the downsampling operator (determined by a vertex partition). More precisely, for a given a variation operator  $\mathbf{M}$  our GFB theory can find a valid  $\mathbf{Q}$  for *any* vertex partition, so that GFBs can be constructed using spectral graph filters of the  $(\mathbf{M}, \mathbf{Q})$ -GFT. Moreover, we show that it is important to optimize these partitions so that they are balanced (Section V) and result in  $\mathbf{Q}$  matrices that are sparse and close to diagonal (Section VI). Our main contributions are summarized next.

**Theory of GFBs (Section IV):** We introduce a new *spectral folding property* for the  $(\mathbf{M}, \mathbf{Q})$ -GFT, analogous to that satisfied by the eigenvectors and eigenvalues of the normalized Laplacian of bipartite graphs [39]. For a given variation operator  $\mathbf{M}$  and a vertex partition for downsampling, we show that there exists a unique inner product matrix  $\mathbf{Q}$  such that the  $(\mathbf{M}, \mathbf{Q})$ -GFT obeys the spectral folding property. Based on this result, we propose perfect reconstruction and  $\mathbf{Q}$ -orthogonal filter banks using spectral graph filters of the  $(\mathbf{M}, \mathbf{Q})$ -GFT. Our conditions in the graph frequency domain are exactly those developed in [10], [11] for the normalized Laplacian of bipartite graphs and therefore we can reuse any of the previously proposed filter designs, including those in [10], [11] and improved solutions such as [12], [13]. When

<sup>1</sup>The use of non traditional Hilbert spaces has proven effective in various studies involving irregularly structured data, such as graph sparsification [33], machine learning [34], compression of 3D point clouds [35], [36], graph signal sampling [37], and perceptual coding [38].

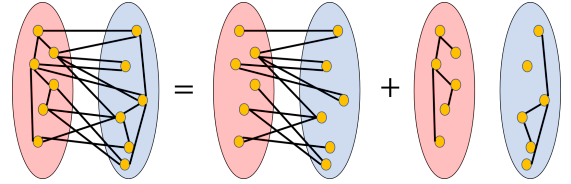


Fig. 2: Representation of a graph (left) as the sum of a bipartite graph (center) and a disconnected graph with 2 or more connected components (right). Red and blue circles contain node sets  $\mathcal{A}$  and  $\mathcal{B}$ , respectively.

$\mathbf{M}$  is the normalized Laplacian and the graph is bipartite, we recover the BFB framework.

In our preliminary version of this work [40] we introduced the spectral folding property and two-channel filter banks on arbitrary graphs (Sections IV-D and IV-F), while an application of GFBs to image compression has been recently published [28]. In this paper, we further develop the GFB theory, providing all proofs not given in [40], discussing the results in more depth and introducing the following novel contributions.

**Properties, interpretations and examples (Section V):** Since  $(\mathbf{M}, \mathbf{Q})$ -GFTs are relatively new, especially when  $\mathbf{Q}$  is not diagonal, Section V is devoted to studying their properties. We show that some spectral properties of the normalized and random walk Laplacians can be extended to the proposed  $(\mathbf{M}, \mathbf{Q})$ -GFTs. We also provide examples of  $(\mathbf{M}, \mathbf{Q})$ -GFTs with and without the spectral folding property (Figure 6). Representing an arbitrary graph as the sum of a bipartite and a disconnected graph (Figure 2) leads to a vertex domain interpretation of the proposed spectral graph filters. Finally, we use Gaussian graphical models to give a probabilistic interpretation of GFBs and the spectral folding property.

**Vertex partitioning (Section VI):** While the GFB theory is valid for arbitrary vertex partitions, not all vertex partitions are desirable for downsampling. As an example, in Section V we prove that unbalanced vertex partitions lead to GFBs with poor frequency selectivity, and thus balanced partitions should be used. In Section VI we propose a numerical stability criterion for vertex set partition along with a computationally efficient algorithm based on an approximate solution to a maximum cut (max-cut) problem. Essentially, our algorithm finds vertex partitions leading to a graph decomposition (Figure 2) where the bipartite part has the largest cut, while the disconnected graph is sparse and has small weights, which is also helpful to reduce the complexity of GFB implementations. Note that bipartite approximation algorithms for BFBs have been formulated as max-cut problems [23]. However, these approach result in the removal of non-bipartite edges, while in our case edge removal is unnecessary.

In this paper, the inner product defined by  $\mathbf{Q}$  plays a fundamental role: It not only leads to a definition of the  $(\mathbf{M}, \mathbf{Q})$ -GFT and to conditions for  $\mathbf{Q}$ -orthogonal filter banks, but it is also needed to understand biorthogonal designs (i.e., good biorthogonal filters are such that they are approximately  $\mathbf{Q}$ -orthogonal). Since the choice  $\mathbf{Q} = \mathbf{I}$  is the dominant one in both signal processing and GSP, it is important to understand the implications of not using the standard ( $\mathbf{Q} = \mathbf{I}$ )

inner product. To address this point, note that relaxing the  $\mathbf{I}$ -orthogonality requirement is often an option if it is necessary to achieve some desirable properties. As an example JPEG2000 uses biorthogonal filters that are nearly  $\mathbf{I}$ -orthogonal because they have finite support and are symmetric, which is desirable for imaging applications and would not be possible with orthogonal filters. Similarly, biorthogonal filter banks on bipartite graphs are preferred over  $\mathbf{I}$ -orthogonal ones because they have polynomial implementations [11]. Thus, in practice a non  $\mathbf{I}$ -orthogonal solution can be useful as long as it is sufficient close to being  $\mathbf{I}$ -orthogonal. In this work, we use biorthogonal filters (obtained from [11]) that lead to polynomial filters and can be designed to be nearly  $\mathbf{Q}$ -orthogonal (see Section IV). Additionally, in Section VI we show that the downsampling operator can be optimized so that the  $\mathbf{Q}$  matrices have favorable properties (sparsity, close to diagonal and with small condition number in operator norm) so that the  $\mathbf{Q}$  inner product approximates the conventional dot product. How closely the best  $\mathbf{Q}$  matrix for a given graph approximates the dot product depends on the graph itself (degree irregularity, sparsity, etc), but we show examples for specific graphs (sensor network, spatial graphs, and 3D point cloud graphs) showing that good approximations can be achieved. Further analysis of this question for more general scenarios is left for future work.

The rest of the paper is organized as follows. In Section II we review related work. In Section III we introduce the fundamentals of GSP on general Hilbert spaces, while Section IV is dedicated to bipartite and generalized filter banks. Section V focuses on properties of  $(\mathbf{M}, \mathbf{Q})$ -GFTs and GFBs. Section VI studies optimal vertex partitioning for downsampling. We end this paper with numerical results, and conclusions in Sections VII and VIII respectively. Additional proofs can be found in the Appendix.

## II. RELATED WORK

We discuss related filter banks and multiresolution representations (MRR) on graphs from three perspectives: graph topology, graph matrix, and downsampling sets.

**Graph topology.** Several existing filter bank theories are applicable only to graphs with certain types of topology such as: bipartite [10], [11],  $M$ -block cyclic [41], [42], circulant [48], and acyclic [49]. While some of these graph structures appear naturally in some applications [50], [51], many cases graphs of interest do not belong to any of these categories. To apply BFBs to arbitrary graphs one can decompose any graph as a sum of bipartite graphs and apply the filter bank in a separable manner [52]. Other approaches include bipartite approximation [23], bipartite graph learning methods [24]–[27], [53], graph oversampling [43], and vertex partition optimization [54]. Earlier filter bank designs for arbitrary graphs are difficult to invert (e.g., least squares reconstruction is needed) [55]–[57]. More recent MRRs fail to be simultaneously perfect reconstruction and orthogonal [44], while others, require full eigendecomposition [45], [58]. Existing approaches that are valid for arbitrary graphs have several disadvantages. On the one hand, approximation-based methods may reduce signal

representation quality while also requiring additional computational resources (to select the best bipartite approximation) [23]–[25], [52]. On the other hand, methods that allow the original graph to be used can do so at the expense of other desirable features, such as low complexity [45], [58], perfect reconstruction or orthogonality (in  $\mathbf{I}$  or other  $\mathbf{Q}$  inner product) [44], [54] (see Table I for a comparison of some of these approaches). Therefore, a theoretical formulation leading to critically sampled filter banks for arbitrary graphs, without the aforementioned disadvantages, can be an attractive alternative.

**Graph matrix.** The choice of graph matrix, such as the graph Laplacian or the adjacency matrix, whose non-zero pattern encodes the graph structure, is an important design decision [59], [60]. Existing filter bank frameworks are built for specific types of graph matrices because of their special algebraic or spectral properties [10], [41], but these choices may not be suitable for a particular application. As an example, BFBs use the normalized Laplacian [10], while the random walk Laplacian has been shown to achieve better coding performance [28]. More recent filter bank approaches [46], [47] can be applied to the larger class of positive semi-definite variation operators. However, they lack perfect reconstruction [46] or require computing a full eigendecomposition of the graph operator [47], which significantly limits their application to large graphs. The proposed GFBs are valid for any positive semi definite graph matrix (i.e., a variation operator), including commonly used graph Laplacians, without compromising on other properties.

**Downsampling.** For discrete-time signals, a downsampling by 2 operator keeps “every other sample” and discards the rest. In graphs, there is no obvious notion of “every other vertex” unless the graph is bipartite [52]. For graph filter banks, vertex partitions of the node set can be chosen under various criteria [9], [46], [54]. Recently, [47], [61] used spectral domain sampling, and while this approach leads to an attractive theory, spectral sampling requires computing all eigenvectors and eigenvalues of the graph matrix, which can have significant computation complexity. [46] extended sampling theory of graph signals to filter banks but practical implementations of this framework cannot achieve perfect reconstruction. In this work, we show that any partition of the vertex set is a valid downsampling operator. We also propose strategies for optimally choosing these partitions in Section VI.

## III. GSP IN GENERAL HILBERT SPACES

### A. Notation

Scalars, vectors and matrices are written in lower case regular, lower case bold and upper case bold respectively (e.g.,  $a$ ,  $\mathbf{b}$ ,  $\mathbf{C}$ ). Positive definite and semi-definite matrices are denoted by  $\mathbf{A} \succ 0$ , and  $\mathbf{A} \succeq 0$  respectively. We will denote by  $\mathbf{C}_{AB}$ , the sub-matrix of  $\mathbf{C}$  whose rows and columns are indexed by the sets  $\mathcal{A}$  and  $\mathcal{B}$ , respectively. The spectral norm or largest singular value of a matrix  $\mathbf{A}$  is denoted by  $\|\mathbf{A}\|$ .

### B. Graph signal processing

Consider a graph  $\mathcal{G} = (\mathcal{V}, \mathcal{E})$  with vertex set  $\mathcal{V} = \{1, \dots, n\}$ , and edge set  $\mathcal{E} \subset \mathcal{V} \times \mathcal{V}$ . A graph signal is a

Ref.	PR	O	Poly.	Crit. Samp.	AO	SO	Graph Type	Graph Matrix
Laplacian BFB [10]	✓	✓(I)	✗	✓	SGF	SGF	Bipartite	$\mathcal{L}$
Biorthogonal Laplacian BFB [11]	✓	✗	✓	✓	SGF	SGF	Bipartite	$\mathcal{L}$
M channel FB [41], [42]	✓	✗	✓	✓	SGF	SGF	M block cyclic	$\mathcal{W}$
Polyphase adjacency BFB [13], [22]	✓	✓(I)	✓	✓	SGF	SGF	Bipartite	$\mathcal{W}$
Oversampled FB [43]	✓	✗	✓	✗	SGF	SGF	Any	$\mathcal{L}$
Graph Pyramid [44]	✓	✗	✓	✗	SGF	pinv	Any	$\mathcal{M}$
Ideal filter FB [45]	✓	✓(I)	✗	✓	SGF	Interp	Any	Any
Approximate ideal filter FB [46]	✗	✗	✓	✓	SGF	Interp	Any	$\mathcal{M}$
Spectral Sampling FB [47]	✓	✓(I)	✗	✓	SGF	SGF	Any	Any
Generalized Filter Banks (GFB)	✓	✓(Q)	✓(Z)	✓	SGF	SGF	Any	$\mathcal{M}$

TABLE I: Comparison of multiresolution representations for graph signals. Transform properties: perfect reconstruction (PR), orthogonal (O) in  $\mathbf{Q}$  or  $\mathbf{I}$  inner product, polynomial filter (Poly), critical sampling (CS), analysis operator (AO), synthesis operator (SO), graph type (GT), and graph operator (GO). Analysis operators are implemented with spectral graph filters (SGF), while synthesis operators may be implemented via pseudo inverse (pinv), interpolation (Interp), or a SGF.

function  $x : \mathcal{V} \rightarrow \mathbb{R}$ , which can be represented by a vector  $\mathbf{x} = [x_1, \dots, x_n]^\top$ , and  $x_i$  is the signal value at vertex  $i \in \mathcal{V}$ .

1) *Graph signal variation*: The graph is equipped with a symmetric positive semi definite variation matrix  $\mathbf{M} = (m_{ij})$ , with sparsity pattern determined by the edge set, that is,  $m_{ij} = m_{ji} = 0$  when  $(i, j) \notin \mathcal{E}$  and  $i \neq j$ . Throughout the paper we will assume that the graph is connected<sup>2</sup> and thus  $\mathbf{M}$  is an irreducible matrix [62], [63]. The graph signal variation is

$$\Delta(\mathbf{x}) = \mathbf{x}^\top \mathbf{M} \mathbf{x}. \quad (1)$$

Intuitively, given two signals of equal energy, the one with larger variation is the one with higher energy in the higher frequencies of the spectrum. Popular choices of variation operator are the normalized, combinatorial and generalized Laplacian matrices [63], which we define next.

The adjacency matrix is a non negative symmetric matrix  $\mathbf{W} = (w_{ij})$ , where  $w_{ij} = 0$ , whenever  $(i, j) \notin \mathcal{E}$ . The degree of node  $i$  is  $d_i = \sum_{j \in \mathcal{V}} w_{ij}$ , and the degree matrix is  $\mathbf{D} = \text{diag}(d_1, \dots, d_n)$ . The *combinatorial graph Laplacian* (CGL) is  $\mathbf{L} = \mathbf{D} - \mathbf{W}$ , while the *normalized graph Laplacian* (NGL) is  $\mathcal{L} = \mathbf{D}^{-1/2} \mathbf{L} \mathbf{D}^{-1/2} = \mathbf{I} - \mathbf{D}^{-1/2} \mathbf{W} \mathbf{D}^{-1/2}$ . A *generalized graph Laplacian* (GGL) is any positive semidefinite matrix with non positive off diagonal entries, which includes the normalized and combinatorial graph Laplacian matrices [63]–[66]. Other variation operators are listed in [29], [67].

2) *The  $(\mathbf{M}, \mathbf{Q})$ -GFT [29]*: Given a positive definite matrix  $\mathbf{Q}$ , we define the  $\mathbf{Q}$  inner product between  $\mathbf{x}$  and  $\mathbf{y}$ , as

$$\langle \mathbf{x}, \mathbf{y} \rangle_{\mathbf{Q}} = \mathbf{y}^\top \mathbf{Q} \mathbf{x}, \quad (2)$$

with induced  $\mathbf{Q}$ -norm  $\|\mathbf{x}\|_{\mathbf{Q}} = \sqrt{\langle \mathbf{x}, \mathbf{x} \rangle_{\mathbf{Q}}}$ . We say  $\{\mathbf{u}_k\}_{k=1}^n$  is a  $\mathbf{Q}$ -orthonormal set if it satisfies

$$\langle \mathbf{u}_i, \mathbf{u}_j \rangle_{\mathbf{Q}} = \begin{cases} 1 & \text{if } i = j \\ 0 & \text{if } i \neq j. \end{cases} \quad (3)$$

In matrix form this corresponds to  $\mathbf{U}^\top \mathbf{Q} \mathbf{U} = \mathbf{I}$ , where  $\mathbf{U} = [\mathbf{u}_1, \dots, \mathbf{u}_n]$ , which also implies that  $\mathbf{U}^{-1} = \mathbf{U}^\top \mathbf{Q}$ . Following [29], the  $(\mathbf{M}, \mathbf{Q})$  *Graph Fourier Transform* ( $(\mathbf{M}, \mathbf{Q})$ -GFT) is defined as the  $\mathbf{Q}$ -orthonormal set that minimizes the graph signal variation, that is

$$\mathbf{u}_1 = \arg \min_{\mathbf{u}: \mathbf{u} \neq \mathbf{0}, \|\mathbf{u}\|_{\mathbf{Q}}=1} \mathbf{u}^\top \mathbf{M} \mathbf{u}, \quad (4)$$

<sup>2</sup>If the graph is disconnected, each connected component can be treated independently.

and for any  $2 \leq k \leq n$

$$\mathbf{u}_k = \arg \min_{\mathbf{u}: \mathbf{u} \neq \mathbf{0}, \|\mathbf{u}\|_{\mathbf{Q}}=1} \mathbf{u}^\top \mathbf{M} \mathbf{u} \text{ s.t. } \langle \mathbf{u}, \mathbf{u}_i \rangle_{\mathbf{Q}} = 0, \forall i < k. \quad (5)$$

Note that this definition of the  $(\mathbf{M}, \mathbf{Q})$ -GFT basis is consistent with the traditional definition of GFT (i.e., the  $(\mathbf{M}, \mathbf{I})$ -GFT). In particular, when  $\mathbf{M} = \mathbf{L}$ , the variation of  $\mathbf{x}$  is  $\mathbf{x}^\top \mathbf{L} \mathbf{x} = \sum_{(i,j) \in \mathcal{E}} w_{ij} (x_i - x_j)^2$ , and as in that case, the generalized eigenvectors  $\mathbf{u}_k$  have increasing variation (quantified with the same operator  $\mathbf{M}$ ) for larger  $k$ . The only difference is that now the basis vectors are  $\mathbf{Q}$ -orthonormal instead of  $\mathbf{I}$ -orthonormal.

The  $(\mathbf{M}, \mathbf{Q})$ -GFT is also the solution to the generalized eigendecomposition problem [29], [62]:

$$\mathbf{M} \mathbf{u} = \lambda \mathbf{Q} \mathbf{u}. \quad (6)$$

The matrix of unit  $\mathbf{Q}$ -norm generalized eigenvectors is denoted by  $\mathbf{U} = [\mathbf{u}_1, \dots, \mathbf{u}_n]$ , with generalized eigenvalues (or graph frequencies) forming a set  $\sigma(\mathbf{M}, \mathbf{Q}) = \{\lambda_1, \dots, \lambda_n\}$  where  $\lambda_k = \mathbf{u}_k^\top \mathbf{M} \mathbf{u}_k$  and  $\lambda_1 \leq \lambda_2 \leq \dots \leq \lambda_n$ . The generalized eigenvalue matrix is  $\mathbf{\Lambda} = \text{diag}(\lambda_1, \dots, \lambda_n)$ . The *fundamental matrix* is  $\mathbf{Z} = \mathbf{Q}^{-1} \mathbf{M}$ , which is diagonalized by  $\mathbf{U}$ , so

$$\mathbf{Z} = \mathbf{Q}^{-1} \mathbf{M} = \mathbf{U} \mathbf{\Lambda} \mathbf{U}^{-1} = \mathbf{U} \mathbf{\Lambda} \mathbf{U}^\top \mathbf{Q}. \quad (7)$$

Then we can factorize the variation operator  $\mathbf{M}$  as follows:

$$\mathbf{M} = \mathbf{Q} \mathbf{U} \mathbf{\Lambda} \mathbf{U}^\top \mathbf{Q}. \quad (8)$$

A graph signal  $\mathbf{x}$  has a  $(\mathbf{M}, \mathbf{Q})$ -GFT representation given by:

$$\mathbf{x} = \sum_{i=1}^n \langle \mathbf{x}, \mathbf{u}_i \rangle_{\mathbf{Q}} \mathbf{u}_i = \mathbf{U} \hat{\mathbf{x}}, \quad (9)$$

where  $\hat{\mathbf{x}} = \mathbf{U}^\top \mathbf{Q} \mathbf{x}$  is the  $(\mathbf{M}, \mathbf{Q})$ -GFT of  $\mathbf{x}$  [29]. Thus, (9) is the inverse  $(\mathbf{M}, \mathbf{Q})$ -GFT, where  $\mathbf{x}$  is reconstructed as a linear combination of the frequency components in  $\hat{\mathbf{x}}$ . Note that the inverse transform is given by  $\mathbf{x} = \mathbf{U} \hat{\mathbf{x}}$ , since  $\mathbf{U} \mathbf{U}^\top \mathbf{Q} = \mathbf{I}$ .

3) *Spectral graph filters*: Given a function (i.e., a filter kernel)  $h : \sigma(\mathbf{M}, \mathbf{Q}) \rightarrow \mathbb{R}$ , then a *spectral graph filter* (SGF) is any matrix  $\mathbf{H}$  of the form

$$\mathbf{H} = \mathbf{U} h(\mathbf{\Lambda}) \mathbf{U}^\top \mathbf{Q} = h(\mathbf{Z}), \quad (10)$$

where  $h(\mathbf{\Lambda}) = \text{diag}(h(\lambda_1), h(\lambda_2), \dots, h(\lambda_n))$ . When  $h(\lambda) = \lambda$  we have that  $\mathbf{H} = \mathbf{Z} = \mathbf{Q}^{-1} \mathbf{M}$  and we recover the fundamental matrix. A spectral graph filter is implemented by

first applying the  $(\mathbf{M}, \mathbf{Q})$ -GFT to a signal  $\mathbf{x}$ , then multiplying each transformed coefficient  $\hat{x}_i = \langle \mathbf{x}, \mathbf{u}_i \rangle_{\mathbf{Q}}$  by the filter coefficient  $h(\lambda_i)$ . The resulting signal is transformed back to the vertex domain with the inverse  $(\mathbf{M}, \mathbf{Q})$ -GFT. Filtering  $\mathbf{x}$  using  $h$  produces the graph signal  $\mathbf{H}\mathbf{x}$ , since

$$\mathbf{H}\mathbf{x} = \mathbf{U}h(\Lambda)\hat{\mathbf{x}} = \sum_{i=1}^n h(\lambda_i)\hat{x}_i\mathbf{u}_i. \quad (11)$$

When  $h$  is a polynomial  $h(\lambda) = a_0 + a_1\lambda + \dots + a_d\lambda^d$  for  $d \in \mathbb{N}$ , the resulting SGF is a polynomial of  $\mathbf{Z}$ , thus  $\mathbf{H} = h(\mathbf{Z}) = a_0\mathbf{I} + a_1\mathbf{Z} + \dots + a_d\mathbf{Z}^d$ , can be implemented efficiently without eigendecomposition using matrix vector products. Thus, if  $\mathbf{Z}$  is sparse and  $d$  is relatively small, graph filtering with polynomial SGFs can be applied efficiently on large graphs. Complexity of polynomial graph filters and filter banks is reviewed in more detail in [Section VI](#).

### C. Vertex and frequency domain Hilbert spaces

Both a graph signal,  $\mathbf{x}$ , and its  $(\mathbf{M}, \mathbf{Q})$ -GFT,  $\hat{\mathbf{x}}$ , can be represented by vectors in  $\mathbb{R}^n$ . However, in our formulation they belong to different Hilbert spaces, namely,  $(\mathbb{R}^n, \langle \cdot, \cdot \rangle_{\mathbf{Q}})$  for  $\mathbf{x}$  and  $(\mathbb{R}^n, \langle \cdot, \cdot \rangle_{\mathbf{I}})$  for  $\hat{\mathbf{x}}$ , where  $\langle \cdot, \cdot \rangle_{\mathbf{I}}$  is the traditional dot product. Thus, we can view the  $(\mathbf{M}, \mathbf{Q})$ -GFT,  $\mathbf{U}^{\top}\mathbf{Q}$ , as a mapping from  $(\mathbb{R}^n, \langle \cdot, \cdot \rangle_{\mathbf{Q}})$  to  $(\mathbb{R}^n, \langle \cdot, \cdot \rangle_{\mathbf{I}})$ , while the inverse  $(\mathbf{M}, \mathbf{Q})$ -GFT  $\mathbf{U}$  is a mapping from  $(\mathbb{R}^n, \langle \cdot, \cdot \rangle_{\mathbf{I}})$  to  $(\mathbb{R}^n, \langle \cdot, \cdot \rangle_{\mathbf{Q}})$ . Making explicit the Hilbert spaces involved in this mapping allows us to state the following property.

**Theorem 1** (Parseval [29]). *Let  $\mathbf{x}, \mathbf{y} \in \mathbb{R}^n$ , and let  $\hat{\mathbf{x}}$  and  $\hat{\mathbf{y}}$  be their respective frequency domain representations, then*

$$\langle \mathbf{x}, \mathbf{y} \rangle_{\mathbf{Q}} = \langle \hat{\mathbf{x}}, \hat{\mathbf{y}} \rangle_{\mathbf{I}}. \quad (12)$$

From (10) it is clear that SGFs are functions from  $(\mathbb{R}^n, \langle \cdot, \cdot \rangle_{\mathbf{Q}})$  to the same Hilbert space. For the rest of the paper we will use the  $\mathbf{Q}$  inner product for graph signals, and the  $\mathbf{I}$  inner product for their frequency domain representations.

## IV. TWO-CHANNEL FILTER BANKS ON GRAPHS

In this section we introduce the two-channel filter bank theory for arbitrary graphs. In [Section IV-A](#) we formulate the problem. [Section IV-B](#) reviews the solution for bipartite graphs from [10]. We illustrate how to go from bipartite to arbitrary graphs through an example in [Section IV-C](#). Our main theoretical result, the generalized spectral folding property is presented in [Section IV-D](#). Generalized filter banks are constructed in [Section IV-F](#) and [Section IV-G](#).

### A. Problem formulation

A two-channel filter bank ([Figure 1](#)) is composed of downsampling and upsampling operators on the sets  $\mathcal{A}$  and  $\mathcal{B}$ , and two sets of  $|\mathcal{V}| \times |\mathcal{V}|$  matrices, corresponding to the analysis filters  $(\mathbf{H}_0, \mathbf{H}_1)$  and the synthesis filters  $(\mathbf{G}_0, \mathbf{G}_1)$ . Throughout the paper, we will consider critically sampled filter banks.

**Definition 1.** *A two-channel filter bank is **critically sampled** if the downsampling sets  $\mathcal{A}$  and  $\mathcal{B}$  form a partition of  $\mathcal{V}$ .*

Without loss of generality we assume that  $\mathcal{A} = \{1, \dots, |\mathcal{A}|\}$ , and  $\mathcal{B} = \mathcal{V} \setminus \mathcal{A}$ . Downsampling  $\mathbf{x}$  on  $\mathcal{A}$  keeps the entries  $\{x_i : i \in \mathcal{A}\}$  and discards the rest, resulting in

$$\mathbf{x}_{\mathcal{A}} = \mathbf{S}_{\mathcal{A}}\mathbf{x}, \quad (13)$$

where  $\mathbf{S}_{\mathcal{A}} = [\mathbf{I}_{\mathcal{A}}, \mathbf{0}]$  is a  $|\mathcal{A}| \times |\mathcal{V}|$  selection matrix. The upsampling operator  $\mathbf{S}_{\mathcal{A}}^{\top}$  maps the signal back to  $\mathcal{V}$  by filling the entries on  $\mathcal{B}$  with zeroes. Downsampling followed by upsampling corresponds to

$$\mathbf{S}_{\mathcal{A}}^{\top}\mathbf{S}_{\mathcal{A}}\mathbf{x} = \mathbf{S}_{\mathcal{A}}^{\top}\mathbf{x}_{\mathcal{A}} = [\mathbf{x}_{\mathcal{A}}^{\top} \quad \mathbf{0}]^{\top}. \quad (14)$$

The analysis operator  $\mathbf{T}_a$  (i.e., filtering followed by downsampling) from [Figure 1](#) can be written as

$$\mathbf{T}_a = \mathbf{S}_{\mathcal{A}}^{\top}\mathbf{S}_{\mathcal{A}}\mathbf{H}_0 + \mathbf{S}_{\mathcal{B}}^{\top}\mathbf{S}_{\mathcal{B}}\mathbf{H}_1 = \begin{bmatrix} \mathbf{S}_{\mathcal{A}}\mathbf{H}_0 \\ \mathbf{S}_{\mathcal{B}}\mathbf{H}_1 \end{bmatrix}. \quad (15)$$

The outputs of the low pass and high pass channels, approximation,  $\mathbf{a}$ , and detail,  $\mathbf{d}$ , coefficients, respectively, are

$$\mathbf{T}_a\mathbf{x} = [\mathbf{a}^{\top} \quad \mathbf{d}^{\top}]^{\top} = [(\mathbf{S}_{\mathcal{A}}\mathbf{H}_0\mathbf{x})^{\top} \quad (\mathbf{S}_{\mathcal{B}}\mathbf{H}_1\mathbf{x})^{\top}]^{\top}. \quad (16)$$

The synthesis operator can be expressed as

$$\mathbf{T}_s = \mathbf{G}_0\mathbf{S}_{\mathcal{A}}^{\top}\mathbf{S}_{\mathcal{A}} + \mathbf{G}_1\mathbf{S}_{\mathcal{B}}^{\top}\mathbf{S}_{\mathcal{B}} = [\mathbf{G}_0\mathbf{S}_{\mathcal{A}}^{\top} \quad \mathbf{G}_1\mathbf{S}_{\mathcal{B}}^{\top}]. \quad (17)$$

Both the analysis and synthesis operators map signals from  $(\mathbb{R}^n, \langle \cdot, \cdot \rangle_{\mathbf{Q}})$  to  $(\mathbb{R}^n, \langle \cdot, \cdot \rangle_{\mathbf{Q}})$  (see also [Section III-C](#)), thus  $\mathbf{x}$ ,  $\mathbf{T}_a\mathbf{x}$ , and  $\mathbf{T}_s\mathbf{T}_a\mathbf{x}$  are vertex domain signals. We are interested in perfect reconstruction two-channel filter banks.

**Definition 2.** *A two-channel filter bank is **perfect reconstruction (PR)** if  $\mathbf{T}_s\mathbf{T}_a\mathbf{x} = \mathbf{x}$ , for all  $\mathbf{x}$ .*

Since we only consider critically sampled filter banks, the PR condition is equivalent to  $\mathbf{T}_s = \mathbf{T}_a^{-1}$ , thus a necessary and sufficient condition for perfect reconstruction is given by

$$\mathbf{T}_s\mathbf{T}_a = \mathbf{G}_0\mathbf{S}_{\mathcal{A}}^{\top}\mathbf{S}_{\mathcal{A}}\mathbf{H}_0 + \mathbf{G}_1\mathbf{S}_{\mathcal{B}}^{\top}\mathbf{S}_{\mathcal{B}}\mathbf{H}_1 = \mathbf{I}. \quad (18)$$

We also introduce  $\mathbf{Q}$ -orthogonal filter banks.

**Definition 3.** *A two-channel filter bank is **Q-orthogonal**, if for every pair of graph signals  $\mathbf{x}, \mathbf{y}$ ,*

$$\langle \mathbf{x}, \mathbf{y} \rangle_{\mathbf{Q}} = \langle \mathbf{T}_a\mathbf{x}, \mathbf{T}_a\mathbf{y} \rangle_{\mathbf{Q}}. \quad (19)$$

*In matrix form, (19) is equivalent to  $\mathbf{T}_a^{\top}\mathbf{Q}\mathbf{T}_a = \mathbf{Q}$ .*

The traditional notion of orthogonal filter banks corresponds to the case  $\mathbf{Q} = \mathbf{I}$ . Critically sampled  $\mathbf{Q}$ -orthogonal filter banks are always perfect reconstruction with synthesis operator

$$\mathbf{T}_s = \mathbf{Q}^{-1}\mathbf{T}_a^{\top}\mathbf{Q}. \quad (20)$$

It is easy to verify that (20) also obeys  $\mathbf{T}_s^{\top}\mathbf{Q}\mathbf{T}_s = \mathbf{Q}$ .

**Remark 1.** *Because the vertex domain and frequency domain Hilbert spaces are different (see [Section III-C](#)),  $\mathbf{Q}$ -orthogonality for filter banks is different than  $\mathbf{Q}$ -orthogonality of the  $(\mathbf{M}, \mathbf{Q})$ -GFT. This is because the  $(\mathbf{M}, \mathbf{Q})$ -GFT maps graph signals from their vertex domain representation to their frequency domain representation, that is,  $\mathbf{U}^{\top}\mathbf{Q} : (\mathbb{R}^n, \langle \cdot, \cdot \rangle_{\mathbf{Q}}) \rightarrow (\mathbb{R}^n, \langle \cdot, \cdot \rangle_{\mathbf{I}})$ , which results in the relationship of [Theorem 1](#) (see [29]). In contrast, the analysis*

and synthesis operators of a PR critically sampled filter bank stay in the same Hilbert space  $(\mathbb{R}^n, \langle \cdot, \cdot \rangle_{\mathbf{Q}})$ .

We seek two-channel filter banks that can provide good signal representations, while having efficient implementations on large (arbitrary) graphs. In practice, this can be achieved by designing SGFs  $\mathbf{H}_i, \mathbf{G}_i$  that: (i) have good frequency selectivity and (ii) can be written as polynomials of  $\mathbf{Z}$ . We review bipartite graph solutions [10], [11] before introducing our proposed GFBs for arbitrary graphs.

### B. Bipartite filter banks [10], [11]

The necessary and sufficient filter bank design conditions of [10], [11] apply to bipartite graphs.

**Definition 4** (Bipartite graph [39]). A graph  $\mathcal{G} = (\mathcal{V}, \mathcal{E})$  is bipartite on a partition of the node set  $\mathcal{A}, \mathcal{B}$ , if for all  $(i, j) \in \mathcal{E}$ ,  $i \in \mathcal{A}$  and  $j \in \mathcal{B}$ , or  $i \in \mathcal{B}$  and  $j \in \mathcal{A}$ .

Some examples of bipartite graphs include Figure 2 (middle graph), Figure 5a and Figure 7b. In bipartite filter banks (BFB) the sets  $\mathcal{A}$  and  $\mathcal{B}$  are used for downsampling. In a bipartite graph only edges between  $\mathcal{A}$  and  $\mathcal{B}$  exist, so we have:

$$\mathbf{L} = \begin{bmatrix} \mathbf{D}_{\mathcal{A}} & -\mathbf{W}_{\mathcal{A}\mathcal{B}} \\ -\mathbf{W}_{\mathcal{B}\mathcal{A}} & \mathbf{D}_{\mathcal{B}} \end{bmatrix}, \quad \mathcal{L} = \begin{bmatrix} \mathbf{I}_{\mathcal{A}} & -\tilde{\mathbf{W}}_{\mathcal{A}\mathcal{B}} \\ -\tilde{\mathbf{W}}_{\mathcal{B}\mathcal{A}} & \mathbf{I}_{\mathcal{B}} \end{bmatrix}. \quad (21)$$

BFBs are implemented using spectral graph filters of the  $(\mathcal{L}, \mathbf{I})$ -GFT, that is  $\mathbf{Z} = \mathcal{L}$ , and

$$\mathbf{H}_i = h_i(\mathcal{L}), \quad \mathbf{G}_i = g_i(\mathcal{L}), \quad i \in \{0, 1\}. \quad (22)$$

The diagonal matrix  $\mathbf{J} = \mathbf{S}_{\mathcal{A}}^{\top} \mathbf{S}_{\mathcal{A}} - \mathbf{S}_{\mathcal{B}}^{\top} \mathbf{S}_{\mathcal{B}}$ , with entries

$$\mathbf{J}_{i,i} = \begin{cases} 1 & \text{if } i \in \mathcal{A} \\ -1 & \text{if } i \in \mathcal{B}, \end{cases} \quad (23)$$

is used to establish the following property of the normalized Laplacian of bipartite graphs.

**Proposition 1** (Spectral folding [39]). Let  $\mathcal{L}$  be the normalized Laplacian of a bipartite graph, we have that  $\mathcal{L}\mathbf{u} = \lambda\mathbf{u}$  if and only if  $\mathbf{J}\mathbf{u}$  is also an eigenvector with eigenvalue  $2 - \lambda$ .

Thus, eigenvalues come in pairs  $(\lambda, 2 - \lambda)$  mirrored around the middle frequency  $\lambda = 1$ . For a given  $\lambda$ , the eigenvector  $\mathbf{u}$  and its folded version  $\mathbf{J}\mathbf{u}$  have the same values for entries in  $\mathcal{A}$ , while signs are changed for the entries in  $\mathcal{B}$ . Proposition 1 is the key property used by [10], [11] to design perfect reconstruction and  $\mathbf{I}$ -orthogonal BFBs.

**Theorem 2** (Perfect Reconstruction [10]). A two-channel filter bank on a bipartite graph with spectral graph filters given by (22) is PR if and only if,  $\forall \lambda \in \sigma(\mathcal{L}, \mathbf{I})$

$$g_0(\lambda)h_0(\lambda) + g_1(\lambda)h_1(\lambda) = 2, \quad (24)$$

$$h_1(\lambda)g_1(2 - \lambda) - h_0(\lambda)g_0(2 - \lambda) = 0. \quad (25)$$

The proof follows from using  $\mathbf{S}_{\mathcal{A}}^{\top} \mathbf{S}_{\mathcal{A}} = \frac{1}{2}(\mathbf{I} + \mathbf{J})$  and  $\mathbf{S}_{\mathcal{B}}^{\top} \mathbf{S}_{\mathcal{B}} = \frac{1}{2}(\mathbf{I} - \mathbf{J})$  in the PR condition (18), in combination with Proposition 1 (see [10]). Proposition 1 can also be used to design  $\mathbf{I}$ -orthogonal filter banks.

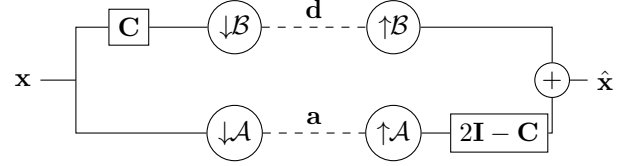


Fig. 3: Lazy two-channel filter bank

**Theorem 3** (Orthogonality [10]). Under the same conditions of Theorem 2, a filter bank is  $\mathbf{I}$ -orthogonal if and only if,  $\forall \lambda \in \sigma(\mathcal{L}, \mathbf{I})$

$$h_0^2(\lambda) + h_1^2(\lambda) = 2, \quad (26)$$

$$h_1(\lambda)h_1(2 - \lambda) - h_0(\lambda)h_0(2 - \lambda) = 0. \quad (27)$$

The main advantage of  $\mathbf{I}$ -orthogonal over non  $\mathbf{I}$ -orthogonal PR filter banks is the energy preservation property (Definition 3), essential for compression and de-noising applications. Because no polynomial solutions to (26) and (27) exist [11],  $\mathbf{I}$ -orthogonal filter banks cannot be implemented with polynomial graph filters. Instead, polynomial biorthogonal filter banks with near  $\mathbf{I}$ -orthogonality can be designed [11].

**Proposition 2.** [11], [13] Biorthogonal filters defined by

$$h_0(\lambda) = g_1(2 - \lambda), \quad h_1(\lambda) = g_0(2 - \lambda), \quad (28)$$

$$h_0(\lambda)h_1(2 - \lambda) + h_0(2 - \lambda)h_1(\lambda) = 2 \quad (29)$$

are perfect reconstruction.

In what follows we will show that the PR,  $\mathbf{I}$ -orthogonality and biorthogonal conditions are not limited to bipartite graphs and the normalized Laplacian. The key insight is a generalization of Proposition 1.

### C. From bipartite to arbitrary graphs: Lazy filter bank

Before stating our main results, we show how our extension from bipartite to arbitrary graphs would work for the “lazy” filter bank of Figure 3, where  $\mathbf{C}$  is given by

$$\mathbf{C} = \begin{bmatrix} \mathbf{I}_{\mathcal{A}} & \mathbf{C}_{\mathcal{A}\mathcal{B}} \\ \mathbf{C}_{\mathcal{B}\mathcal{A}} & \mathbf{I}_{\mathcal{B}} \end{bmatrix}. \quad (30)$$

$\mathbf{C}_{\mathcal{A}\mathcal{B}}$  and  $\mathbf{C}_{\mathcal{B}\mathcal{A}}$  are arbitrary rectangular matrices of dimensions  $|\mathcal{A}| \times |\mathcal{B}|$  and  $|\mathcal{B}| \times |\mathcal{A}|$ , respectively. It is easy to verify that the lazy filter bank is perfect reconstruction when  $\mathbf{C}$  is given by (30). Since  $\mathbf{d} = \mathbf{S}_{\mathcal{B}}\mathbf{C}\mathbf{x}$  and  $\mathbf{a} = \mathbf{S}_{\mathcal{A}}\mathbf{x}$ , we have that

$$\begin{aligned} \hat{\mathbf{x}} &= \mathbf{S}_{\mathcal{B}}^{\top} \mathbf{d} + (2\mathbf{I} - \mathbf{C})\mathbf{S}_{\mathcal{A}}^{\top} \mathbf{a} = (\mathbf{S}_{\mathcal{B}}^{\top} \mathbf{S}_{\mathcal{B}} \mathbf{C} + (2\mathbf{I} - \mathbf{C})\mathbf{S}_{\mathcal{A}}^{\top} \mathbf{S}_{\mathcal{A}})\mathbf{x} \\ &= \left( \begin{bmatrix} \mathbf{0} & \mathbf{0} \\ \mathbf{C}_{\mathcal{B}\mathcal{A}} & \mathbf{I}_{\mathcal{B}} \end{bmatrix} + \begin{bmatrix} \mathbf{I}_{\mathcal{A}} & \mathbf{0} \\ -\mathbf{C}_{\mathcal{B}\mathcal{A}} & \mathbf{0} \end{bmatrix} \right) \mathbf{x} = \mathbf{x}. \end{aligned} \quad (31)$$

If we take  $\mathbf{C} = \mathcal{L}$  for a bipartite graph, the lazy filter bank is a special case of a perfect reconstruction BFB (Figure 1) with filters  $\mathbf{H}_0 = \mathbf{I}$ ,  $\mathbf{H}_1 = \mathcal{L}$ ,  $\mathbf{G}_0 = 2\mathbf{I} - \mathcal{L}$ , and  $\mathbf{H}_1 = \mathbf{I}$ , corresponding to SGFs of the  $(\mathcal{L}, \mathbf{I})$ -GFT with biorthogonal filter kernels  $h_0(\lambda) = g_1(\lambda) = 1$ ,  $h_1(\lambda) = \lambda$ , and  $g_0(\lambda) = h_1(2 - \lambda)$ . In the following subsections we will show that it is also possible to choose  $\mathbf{C}$  as a function of the variation operator  $\mathbf{M}$  of a non-bipartite graph, which allows us to generalize the theorems from Section IV-B to arbitrary graphs.

#### D. Spectral folding on arbitrary graphs

We generalize [Proposition 1](#) to other graphs and variation operators by using the  $\mathbf{Q}$  inner product. Using this result, we propose a new  $(\mathbf{M}, \mathbf{Q})$ -GFT and show that it can be used to obtain *Generalized Filter Banks* on arbitrary graphs. First we define the spectral folding property for a  $(\mathbf{M}, \mathbf{Q})$ -GFT.

**Definition 5** (Spectral folding). *Given a graph  $\mathcal{G}$  with variation operator  $\mathbf{M} \succeq 0$ , inner product  $\mathbf{Q} \succ 0$  and a partition  $\mathcal{A}, \mathcal{B}$ . The  $(\mathbf{M}, \mathbf{Q})$ -GFT has the **spectral folding property**, if for all generalized eigenpairs  $(\mathbf{u}, \lambda)$  then  $(\mathbf{J}\mathbf{u}, (2 - \lambda))$  is also a generalized eigenpair, that is:*

$$\mathbf{M}\mathbf{u} = \lambda\mathbf{Q}\mathbf{u} \Leftrightarrow \mathbf{M}\mathbf{J}\mathbf{u} = (2 - \lambda)\mathbf{Q}\mathbf{J}\mathbf{u}, \quad (32)$$

where  $\mathbf{J} = \mathbf{S}_A^\top \mathbf{S}_A - \mathbf{S}_B^\top \mathbf{S}_B$ , as in [\(23\)](#).

The following theorem completely characterizes the spectral folding property. The proof can be found in [Section IV-E](#).

**Theorem 4** (Spectral folding). *Given a graph  $\mathcal{G}$  with variation operator  $\mathbf{M} \succeq 0$ , inner product  $\mathbf{Q}$  and a partition  $\mathcal{A} = \{1, \dots, |\mathcal{A}|\}$ ,  $\mathcal{B} = \mathcal{V} \setminus \mathcal{A}$ , for which  $\mathbf{M}_{\mathcal{A}\mathcal{A}}$  and  $\mathbf{M}_{\mathcal{B}\mathcal{B}}$  are invertible. The  $(\mathbf{M}, \mathbf{Q})$ -GFT has the spectral folding property if and only if  $\mathbf{Q}$  is chosen as*

$$\mathbf{Q} = \begin{bmatrix} \mathbf{M}_{\mathcal{A}\mathcal{A}} & \mathbf{0} \\ \mathbf{0} & \mathbf{M}_{\mathcal{B}\mathcal{B}} \end{bmatrix}. \quad (33)$$

The condition that  $\mathbf{M}_{\mathcal{A}\mathcal{A}}$  and  $\mathbf{M}_{\mathcal{B}\mathcal{B}}$  are non singular is satisfied for any vertex partition if  $\mathbf{M} \succ 0$ . This condition also holds if  $\mathbf{M}$  is the combinatorial or normalized Laplacian of a connected graph. [Theorem 4](#) generalizes [Proposition 1](#), demonstrating that the spectral folding property is not unique to the  $(\mathcal{L}, \mathbf{I})$ -GFT of bipartite graphs, and in fact, it is always satisfied if the inner product matrix  $\mathbf{Q}$  is chosen as in [\(33\)](#).

Using [\(33\)](#), the fundamental matrix  $\mathbf{Z} = \mathbf{U}\mathbf{\Lambda}\mathbf{U}^\top \mathbf{Q}$  is

$$\mathbf{Z} = \mathbf{Q}^{-1}\mathbf{M} = \begin{bmatrix} \mathbf{I}_A & \mathbf{M}_{\mathcal{A}\mathcal{A}}^{-1}\mathbf{M}_{\mathcal{A}\mathcal{B}} \\ \mathbf{M}_{\mathcal{B}\mathcal{B}}^{-1}\mathbf{M}_{\mathcal{B}\mathcal{A}} & \mathbf{I}_B \end{bmatrix}, \quad (34)$$

so that  $\mathbf{Z}$  has the same structure as  $\mathbf{C}$  in [\(30\)](#) and thus  $\mathbf{Z}$  can be used to construct ‘‘lazy’’ filter banks (see [Figure 3](#)). In [Section IV-F](#) we apply [Theorem 4](#) with the fundamental matrix  $\mathbf{Z}$  in [\(34\)](#) to design GFBs on arbitrary graphs. To gain some intuition about  $(\mathbf{M}, \mathbf{Q})$ -GFTs with spectral folding, we study some of their properties from vertex, spectral and probabilistic perspectives ([Section V](#)) and propose criteria to choose vertex partitions with favorable properties ([Section VI](#)).

#### E. Proof of Theorem 4 (Spectral folding)

First we prove that [\(33\)](#) implies the spectral folding property ([Definition 5](#)). Since  $\mathbf{M}$  and  $\mathbf{Q}$  are positive semidefinite, and  $\mathbf{Q}$  is non singular, there is a full set of generalized eigenvectors [\[62\]](#). Let  $\mathbf{u} = [\mathbf{u}_A^\top, \mathbf{u}_B^\top]^\top$  and  $\mathbf{M}\mathbf{u} = \lambda\mathbf{Q}\mathbf{u}$ , then

$$\mathbf{M}_{\mathcal{A}\mathcal{A}}\mathbf{u}_A + \mathbf{M}_{\mathcal{A}\mathcal{B}}\mathbf{u}_B = \lambda\mathbf{Q}_{\mathcal{A}\mathcal{A}}\mathbf{u}_A, \quad (35)$$

$$\mathbf{M}_{\mathcal{B}\mathcal{A}}\mathbf{u}_A + \mathbf{M}_{\mathcal{B}\mathcal{B}}\mathbf{u}_B = \lambda\mathbf{Q}_{\mathcal{B}\mathcal{B}}\mathbf{u}_B. \quad (36)$$

Set  $\mathbf{v} = \mathbf{J}\mathbf{u} = [\mathbf{u}_A^\top, -\mathbf{u}_B^\top]^\top$ , and using [\(35\)](#) and [\(36\)](#) we get

$$\mathbf{M}\mathbf{v} = \begin{bmatrix} \mathbf{M}_{\mathcal{A}\mathcal{A}}\mathbf{u}_A - \mathbf{M}_{\mathcal{A}\mathcal{B}}\mathbf{u}_B \\ \mathbf{M}_{\mathcal{B}\mathcal{A}}\mathbf{u}_A - \mathbf{M}_{\mathcal{B}\mathcal{B}}\mathbf{u}_B \end{bmatrix} \quad (37)$$

$$= \begin{bmatrix} 2\mathbf{M}_{\mathcal{A}\mathcal{A}}\mathbf{u}_A - \lambda\mathbf{Q}_{\mathcal{A}\mathcal{A}}\mathbf{u}_A \\ \lambda\mathbf{Q}_{\mathcal{B}\mathcal{B}}\mathbf{u}_B - 2\mathbf{M}_{\mathcal{B}\mathcal{B}}\mathbf{u}_B \end{bmatrix} = (2 - \lambda)\mathbf{Q}\mathbf{v}. \quad (38)$$

The second equality is implied by  $\mathbf{M}_{\mathcal{A}\mathcal{A}} = \mathbf{Q}_{\mathcal{A}}$ , and  $\mathbf{M}_{\mathcal{B}\mathcal{B}} = \mathbf{Q}_{\mathcal{B}}$ . To prove the other direction of the equivalence in [Definition 5](#) we set  $\gamma = 2 - \lambda$  and repeat the same steps.

Now, we prove that spectral folding implies [\(33\)](#). Let

$$\mathbf{Q} = \begin{bmatrix} \mathbf{Q}_{\mathcal{A}} & \mathbf{Q}_{\mathcal{A}\mathcal{B}} \\ \mathbf{Q}_{\mathcal{B}\mathcal{A}} & \mathbf{Q}_{\mathcal{B}} \end{bmatrix}. \quad (39)$$

We will first show that  $\mathbf{Q}$  is block diagonal. Using the spectral folding assumption and given two generalized eigenvectors  $\mathbf{u}$  and  $\mathbf{v}$  with unit  $\mathbf{Q}$ -norm, we have that  $\mathbf{J}\mathbf{u}$  and  $\mathbf{J}\mathbf{v}$  are also generalized eigenvectors of unit  $\mathbf{Q}$ -norm. In addition,  $\mathbf{J}\mathbf{u}$  is  $\mathbf{Q}$ -orthogonal to  $\mathbf{J}\mathbf{v}$ , and  $\mathbf{u}$  is  $\mathbf{Q}$ -orthogonal to  $\mathbf{v}$ . Therefore, given the matrix of generalized eigenvectors  $\mathbf{U}$ ,

$$\mathbf{U}^\top (\mathbf{Q} + \mathbf{J}\mathbf{Q}\mathbf{J}) \mathbf{U} = 2\mathbf{I}. \quad (40)$$

We replace the right hand side of [\(40\)](#) with  $2\mathbf{U}^\top \mathbf{Q}\mathbf{U} = 2\mathbf{I}$ . After simplification we obtain  $\mathbf{J}\mathbf{Q}\mathbf{J} = \mathbf{Q}$ , meaning that  $\mathbf{Q}_{\mathcal{A}\mathcal{B}} = \mathbf{0}$ , and  $\mathbf{Q}_{\mathcal{B}\mathcal{A}} = \mathbf{0}$ .

Next, we prove that  $\mathbf{Q}_{\mathcal{A}} = \mathbf{M}_{\mathcal{A}\mathcal{A}}$  and  $\mathbf{Q}_{\mathcal{B}} = \mathbf{M}_{\mathcal{B}\mathcal{B}}$ . Using the spectral folding property, and given  $\mathbf{u}$ , a generalized eigenvector with eigenvalue  $\lambda$ , we obtain:

$$\mathbf{M}(\mathbf{I} + \mathbf{J})\mathbf{u} = (\lambda\mathbf{Q} + (2 - \lambda)\mathbf{Q}\mathbf{J})\mathbf{u} \quad (41)$$

$$\mathbf{M}(\mathbf{I} - \mathbf{J})\mathbf{u} = (\lambda\mathbf{Q} - (2 - \lambda)\mathbf{Q}\mathbf{J})\mathbf{u}. \quad (42)$$

[\(41\)](#) and [\(42\)](#) imply  $2\mathbf{M}_{\mathcal{A}\mathcal{A}}\mathbf{u}_A = 2\mathbf{Q}_{\mathcal{A}}\mathbf{u}_A$  and  $2\mathbf{M}_{\mathcal{B}\mathcal{B}}\mathbf{u}_B = 2\mathbf{Q}_{\mathcal{B}}\mathbf{u}_B$ , respectively. Gathering all these equations for all eigenvectors into matrix form, we obtain  $\begin{bmatrix} \mathbf{M}_{\mathcal{A}\mathcal{A}} & \mathbf{0} \\ \mathbf{0} & \mathbf{M}_{\mathcal{B}\mathcal{B}} \end{bmatrix} \mathbf{U} = \begin{bmatrix} \mathbf{Q}_{\mathcal{A}} & \mathbf{0} \\ \mathbf{0} & \mathbf{Q}_{\mathcal{B}} \end{bmatrix} \mathbf{U}$ . Since  $\mathbf{U}$  is invertible, we obtain that  $\mathbf{M}_{\mathcal{A}\mathcal{A}} = \mathbf{Q}_{\mathcal{A}}$  and  $\mathbf{M}_{\mathcal{B}\mathcal{B}} = \mathbf{Q}_{\mathcal{B}}$ .

#### F. Generalized filter banks on arbitrary graphs

We use the spectral folding property ([Definition 5](#)) and [Theorem 4](#) to construct perfect reconstruction ([Theorem 5](#)) and  $\mathbf{Q}$ -orthogonal ([Theorem 6](#)) filter banks. Our proofs ([Appendices IX-B](#) and [IX-C](#)) follow closely the proofs of [Theorem 2](#) and [Theorem 3](#) for the bipartite case [\[10\]](#), with the main difference being the use of spectral graph filters of the  $(\mathbf{M}, \mathbf{Q})$ -GFT. We state the conditions for perfect reconstruction and  $\mathbf{Q}$ -orthogonal filter banks (see [Definition 3](#)) next.

**Theorem 5.** *Consider a positive semi-definite variation operator  $\mathbf{M}$  and a vertex partition  $\mathcal{A}, \mathcal{B}$ .  $\mathbf{Q}$  is chosen according to [Theorem 4](#) so that the  $(\mathbf{M}, \mathbf{Q})$ -GFT has the spectral folding property. A two-channel filter bank with SGFs*

$$\mathbf{H}_i = h_i(\mathbf{Z}) = \mathbf{U}h_i(\mathbf{\Lambda})\mathbf{U}^\top \mathbf{Q} \text{ and} \quad (43)$$

$$\mathbf{G}_i = g_i(\mathbf{Z}) = \mathbf{U}g_i(\mathbf{\Lambda})\mathbf{U}^\top \mathbf{Q} \quad (44)$$

is perfect reconstruction, if and only if for all  $\lambda \in \sigma(\mathbf{M}, \mathbf{Q})$

$$g_0(\lambda)h_0(\lambda) + g_1(\lambda)h_1(\lambda) = 2, \quad (45)$$

$$h_1(\lambda)g_1(2 - \lambda) - h_0(\lambda)g_0(2 - \lambda) = 0. \quad (46)$$

**Theorem 6.** Under the conditions of [Theorem 5](#), a two-channel filter bank is  $\mathbf{Q}$ -orthogonal if and only if,

$$h_0^2(\lambda) + h_1^2(\lambda) = 2, \quad (47)$$

$$h_1(\lambda)h_1(2-\lambda) - h_0(\lambda)h_0(2-\lambda) = 0, \quad (48)$$

for all  $\lambda \in \sigma(\mathbf{M}, \mathbf{Q})$ .

Note that the PR and  $\mathbf{Q}$ -orthogonality conditions on  $h_i$  and  $g_i$  are the same for BFBs and GFBs. Thus filter designs for BFBs can be used to construct GFBs. From a computational perspective, spectral graph filters that have polynomial filter implementations are more desirable. As in the BFB case, there are no exactly polynomial solutions to the  $\mathbf{Q}$ -orthogonality conditions (47) and (48) [11]. However, the biorthogonal filters from (28) also satisfy the PR conditions of [Theorem 5](#) and have polynomial solutions. Since the biorthogonal designs from [11] are designed to approximately satisfy conditions (47) and (48), they are also approximately  $\mathbf{Q}$ -orthogonal.

**Remark 2.** While  $\mathbf{I}$ -orthogonal filter banks are preferable in many scenarios (e.g., for coding applications), nearly  $\mathbf{I}$ -orthogonal solutions are often used in practice if they provide other useful properties. As an example,  $\mathbf{I}$ -orthogonal filter banks cannot be constructed with finite impulse response linear phase filters (other than the Haar filters) [5], thus nearly  $\mathbf{I}$ -orthogonal biorthogonal filters have been used because of the advantages of symmetry for image coding applications [30]. For GFBs, we will show in [Section VI](#) that by optimizing the downsampling sets based on a numerical stability criteria, the matrix  $\mathbf{Q}$  can be close to a diagonal matrix.

**Remark 3.** The zeroDC filter bank [11] was proposed so that DC (constant) signals are mapped to the lowest graph frequency ( $\lambda = 0$ ). This is achieved by multiplying the input signal by  $\mathbf{D}^{1/2}$  before applying the analysis filter bank (based on the  $(\mathbf{L}, \mathbf{I})$ -GFT), and multiplying by  $\mathbf{D}^{-1/2}$  at the output of the synthesis filter bank. This ensures that a constant input signal has zero response in the high pass channel. [11] showed that biorthogonal zeroDC filter banks can be implemented with polynomials of the random walk Laplacian of a bipartite graph. The zeroDC filter banks can be derived as a special case of our framework with the  $(\mathbf{L}, \mathbf{D})$ -GFT, by noticing that for bipartite graphs with Laplacian  $\mathbf{L}$ , [Theorem 4](#) leads to choosing  $\mathbf{Q} = \mathbf{D}$ .

### G. Tree structured generalized filter banks

Tree structured GFBs are formed by concatenating two-channel GFBs. For all resolution levels, the graphs, variation operators and sampling sets are given and fixed, but otherwise arbitrary. See [Figure 4](#) for an example with  $L = 3$  levels.

We assume the input signal is at resolution  $L$ , thus  $\mathbf{a}_L = \mathbf{x}$ . The outputs of the low and high pass channels at resolution  $\ell < L$  are called approximation and detail coefficients, and are denoted by  $\mathbf{a}_\ell$ , and  $\mathbf{d}_\ell$ , respectively. The sampling sets obey,  $\mathcal{V} = \mathcal{A}_L$ , and for  $\ell < L$ ,  $\mathcal{V}_\ell = \mathcal{A}_\ell$ ,  $\mathcal{A}_{\ell+1} = \mathcal{A}_\ell \cup \mathcal{B}_\ell$ , and  $\mathcal{B}_\ell = \mathcal{A}_{\ell+1} \setminus \mathcal{A}_\ell$ . The graph at resolution  $\ell$  is denoted by  $\mathcal{G}_\ell = (\mathcal{V}_\ell, \mathcal{E}_\ell)$ , and has variation operator  $\mathbf{M}_\ell$  with corresponding

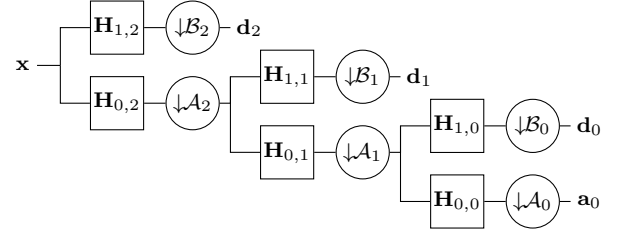


Fig. 4: Tree structured analysis filter bank

inner product matrix  $\mathbf{Q}_\ell$ , chosen so that the  $(\mathbf{M}_\ell, \mathbf{Q}_\ell)$ -GFT has the spectral folding property. We will consider a family of PR filter banks, with analysis and synthesis operators at resolution  $\ell$  denoted by  $\mathbf{T}_{a,\ell}$  and  $\mathbf{T}_{s,\ell} = \mathbf{T}_{a,\ell}^{-1}$ , respectively. The analysis equation at resolution  $\ell$  is given by

$$\mathbf{T}_{a,\ell} \mathbf{a}_{\ell+1} = [\mathbf{a}_\ell^\top \quad \mathbf{d}_\ell^\top]^\top, \quad (49)$$

where  $\mathbf{a}_\ell = \mathbf{S}_{\mathcal{A}_\ell} \mathbf{H}_{0,\ell} \mathbf{a}_{\ell+1}$ , and  $\mathbf{d}_\ell = \mathbf{S}_{\mathcal{B}_\ell} \mathbf{H}_{1,\ell} \mathbf{a}_{\ell+1}$ . The synthesis operator implements

$$\mathbf{a}_{\ell+1} = \mathbf{T}_{s,\ell} [\mathbf{a}_\ell^\top \quad \mathbf{d}_\ell^\top]^\top = \mathbf{G}_{0,\ell} \mathbf{S}_{\mathcal{A}_\ell}^\top \mathbf{a}_\ell + \mathbf{G}_{1,\ell} \mathbf{S}_{\mathcal{B}_\ell}^\top \mathbf{d}_\ell. \quad (50)$$

After applying (50) recursively we can represent  $\mathbf{x}$  as a linear combination of coefficients at various resolutions  $\mathbf{c} = [\mathbf{a}_0^\top, \mathbf{d}_0^\top, \dots, \mathbf{d}_{L-1}^\top]^\top$ , and define the synthesis operator of the tree structured filter bank  $\mathcal{T}_s$  via the equation

$$\mathbf{x} = \mathcal{T}_s \mathbf{c}. \quad (51)$$

Because  $\mathcal{T}_s$  is the composition of the synthesis operators  $\mathbf{T}_{s,\ell}$  at multiple resolutions, there is a corresponding analysis operator  $\mathcal{T}_a = \mathcal{T}_s^{-1}$ , that can be implemented as a composition of analysis operators  $\mathbf{T}_{a,\ell}$ .

## V. PROPERTIES, INTERPRETATION AND EXAMPLES

The term *graph Fourier transform* (GFT) associated to the eigenvectors of a graph operator is often justified by the fact that the discrete Fourier transform (DFT) diagonalizes the adjacency matrix of circulant graphs. More generally, the frequency interpretation of the  $(\mathbf{M}, \mathbf{I})$ -GFT is justified from its variational definition, i.e., (4) and (5). In this section we motivate the use of the proposed  $(\mathbf{M}, \mathbf{Q})$ -GFTs for graph signal representation, provide insights about its frequency interpretation, and through examples help further understand the role of  $\mathbf{Q}$ .

### A. Spectral properties of the $(\mathbf{M}, \mathbf{Q})$ -GFT

1) *Eigenvalue bounds:* For any graph with normalized Laplacian  $\mathcal{L} = \mathbf{D}^{-1/2} \mathbf{L} \mathbf{D}^{-1/2}$ , its eigenvalues belong to the  $[0, 2]$  interval, moreover  $\sigma(\mathbf{L}, \mathbf{D}) = \sigma(\mathcal{L}, \mathbf{I}) \subset [0, 2]$  [39]. Also, for the  $(\mathbf{L}, \mathbf{D})$ -GFT and  $(\mathcal{L}, \mathbf{I})$ -GFT,  $\lambda_n = 2$  if and only if the graph is bipartite [39]. For the  $(\mathbf{M}, \mathbf{Q})$ -GFT there is a similar result.

**Proposition 3.** If the  $(\mathbf{M}, \mathbf{Q})$ -GFT has the spectral folding property then  $\sigma(\mathbf{M}, \mathbf{Q}) \subset [0, 2]$ , and  $\lambda_n = 2$  if and only if  $\lambda_1 = 0$ .



*Proof.* For all  $\mathbf{x}$ ,  $\mathbf{x}^\top \mathbf{M} \mathbf{x} \geq 0$  and  $\mathbf{x}^\top \mathbf{J} \mathbf{M} \mathbf{J} \mathbf{x} \geq 0$ , therefore

$$0 \leq \mathbf{x}^\top \mathbf{M} \mathbf{x} \leq \mathbf{x}^\top \mathbf{M} \mathbf{x} + \mathbf{x}^\top \mathbf{J} \mathbf{M} \mathbf{J} \mathbf{x} = 2\mathbf{x}^\top \mathbf{Q} \mathbf{x}, \quad (52)$$

where we use the identity  $\mathbf{M} + \mathbf{J} \mathbf{M} \mathbf{J} = 2\mathbf{Q}$ . Now for any generalized eigenvector  $\mathbf{u}$  with unit  $\mathbf{Q}$ -norm and eigenvalue  $\lambda$ , we have  $\mathbf{u}^\top \mathbf{M} \mathbf{u} = \lambda \mathbf{u}^\top \mathbf{Q} \mathbf{u} = \lambda$ , and using (52) we obtain

$$0 \leq \frac{\mathbf{u}^\top \mathbf{M} \mathbf{u}}{\mathbf{u}^\top \mathbf{Q} \mathbf{u}} = \lambda \leq 2. \quad (53)$$

The statement,  $\lambda_n = 2$  if and only if  $\lambda_1 = 0$ , follows directly from the spectral folding property.  $\square$

2) *Middle frequency*  $\lambda = 1$ : In the bipartite case, the subspace associated to the eigenvectors corresponding to  $\lambda = 1$  has the least frequency discrimination because energies at this frequency contribute equally to the low pass and high pass channels. This can be seen from (27) evaluated at  $\lambda = 1$ , which shows that  $h_0(1)^2 = h_1(1)^2$ . Since the subspace associated to  $\lambda = 1$  has dimension at least  $\|\mathcal{A}\| - \|\mathcal{B}\|$ , bipartite graphs with more balanced partitions are usually preferred [24]. There is a similar result for the  $(\mathbf{M}, \mathbf{Q})$ -GFT.

**Proposition 4.** *If the  $(\mathbf{M}, \mathbf{Q})$ -GFT has the spectral folding property with vertex partition partition  $\mathcal{A}, \mathcal{B}$ , then the multiplicity of  $\lambda = 1$  is at least  $\|\mathcal{A}\| - \|\mathcal{B}\|$ .*

*Proof.* We will show that

$$|\{i : \lambda_i = 1\}| \geq \|\mathcal{A}\| - \|\mathcal{B}\|. \quad (54)$$

If  $\lambda = 1$ , and  $\mathbf{u}$  is the corresponding generalized eigenvector, then  $\mathbf{Z} \mathbf{u} = \mathbf{u}$ , hence the dimension of the null space of  $\mathbf{I} - \mathbf{Z}$  is equal to the multiplicity of  $\lambda = 1$ . Note that  $\mathbf{I} - \mathbf{Z}$  has a the sparsity pattern of a bipartite adjacency matrix, thus  $(\mathbf{I} - \mathbf{Z})^2$  is block diagonal, and

$$|\{i : \lambda_i = 1\}| = \dim \ker(\mathbf{I} - \mathbf{Z}) \quad (55)$$

$$= n - \text{rank}(\mathbf{Z}_{\mathcal{A}\mathcal{B}}) - \text{rank}(\mathbf{Z}_{\mathcal{B}\mathcal{A}}) \quad (56)$$

$$= n - 2 \text{rank}(\mathbf{M}_{\mathcal{A}\mathcal{B}}) \quad (57)$$

$$\geq n - 2 \min(\|\mathcal{A}\|, \|\mathcal{B}\|) \quad (58)$$

$$= \|\mathcal{A}\| - \|\mathcal{B}\|. \quad (59)$$

The rank of  $\mathbf{I} - \mathbf{Z}$  is the sum of the ranks of the blocks (this can be proven using the fact that  $t(\mathbf{I} - \mathbf{Z})^2$  is block diagonal). Then the rank of each individual term is equal to the rank of  $\mathbf{M}_{\mathcal{A}\mathcal{B}}$ , because  $\mathbf{Q}$  is non-singular. The rank of a matrix is upper bounded by the minimum between the number of rows and columns. Finally we use the fact that  $n = \|\mathcal{A}\| + \|\mathcal{B}\|$ .  $\square$

3) *Multiplicity of  $\lambda_1$* : When  $\mathbf{M}$  is a generalized Laplacian the multiplicity of the smallest eigenvalue is equal to the number of connected components of the graph [63]. The smallest generalized eigenvalue also has this property.

**Proposition 5.** *If  $\mathbf{M} \succeq 0$  is a generalized Laplacian, that is,  $\mathbf{M}_{ij} \leq 0$  for all  $i \neq j$ , the  $(\mathbf{M}, \mathbf{Q})$ -GFT has the spectral folding property, and  $n \geq 2$ , then the multiplicity of  $\lambda_1$  is equal to the number of connected components of the graph.*

*Proof.* Let  $\lambda_1$  be the smallest generalized eigenvalue. The operation  $\hat{\mathbf{M}} = \mathbf{M} - \lambda_1 \mathbf{Q}$  preserves generalized eigenvectors, and shifts all generalized eigenvalues by  $-\lambda_1$ . Then the

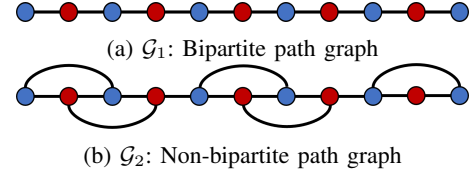
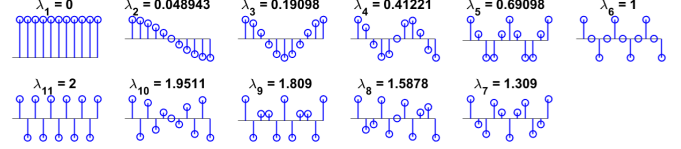
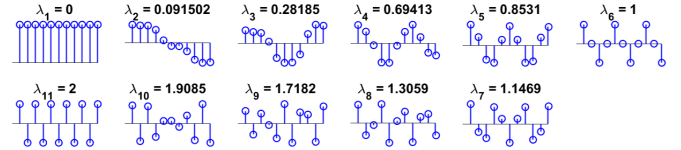


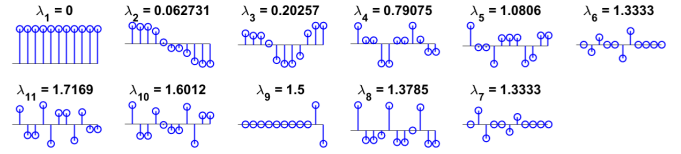
Fig. 5: Examples of two similar path graphs with  $n = 11$  nodes. Vertex partition is marked with blue (nodes in  $\mathcal{A}$ ) and red (nodes in  $\mathcal{B}$ ).



(a) Basis functions of the  $(\mathbf{L}_1, \mathbf{D}_1)$ -GFT of graph  $\mathcal{G}_1$



(b) Basis functions of the  $(\mathbf{L}_2, \mathbf{Q}_2)$ -GFT of graph  $\mathcal{G}_2$



(c) Basis functions of the  $(\mathbf{L}_2, \mathbf{D}_2)$ -GFT of graph  $\mathcal{G}_2$

Fig. 6: Graph Fourier transforms for graphs of Figure 5

multiplicity of  $\lambda_1$  is equal to dimension of the null space of  $\hat{\mathbf{M}}$ , thus the desired result is proven if we can show that  $\hat{\mathbf{M}}$  is a positive semi-definite generalized Laplacian. To show that  $\hat{\mathbf{M}} \succeq 0$ , note (6) implies that  $\hat{\mathbf{M}} = \sum_{i=1}^n (\lambda_i - \lambda_1) \mathbf{Q} \mathbf{u}_i \mathbf{u}_i^\top \mathbf{Q}$ , thus  $\mathbf{x}^\top \hat{\mathbf{M}} \mathbf{x} \geq 0$  for any  $\mathbf{x}$ . To see that  $\hat{\mathbf{M}}$  is also a generalized Laplacian we use the identity

$$\hat{\mathbf{M}} = (1 - \lambda_1) \mathbf{Q} + \mathbf{M} - \mathbf{Q}. \quad (60)$$

Because  $n \geq 2$  and the spectral folding property,  $\lambda_1 \leq 1$ , and  $(1 - \lambda_1) \mathbf{Q}$  is a generalized Laplacian. Since  $\mathbf{M} - \mathbf{Q}$  has zero diagonal and non positive off-diagonal entries, then  $\hat{\mathbf{M}}$  must be a generalized Laplacian.  $\square$

4) *(M, Q)-GFT examples*:  $\mathcal{G}_1$  in Figure 5a is a bipartite path graph, while  $\mathcal{G}_2$  in Figure 5b is a non bipartite graph, formed by adding a few edges to  $\mathcal{G}_1$ . All edge weights in  $\mathcal{G}_1$  and  $\mathcal{G}_2$  are equal to 1. For each graph we use their combinatorial Laplacian  $\mathbf{L}$  as variation operator. The vertex partition is marked by colored vertices, where blue and red correspond to the sets  $\mathcal{A}$  and  $\mathcal{B}$ , respectively. The Laplacian and degree matrices of  $\mathcal{G}_i$  are denoted by  $\mathbf{L}_i$  and  $\mathbf{D}_i$ , respectively. In Figure 6a and Figure 6b we plot the  $(\mathbf{M}, \mathbf{Q})$ -GFTs for graphs  $\mathcal{G}_1$  and  $\mathcal{G}_2$  that have the spectral folding property. Since  $\mathcal{G}_1$

is bipartite, we plot  $(\mathbf{L}_1, \mathbf{D}_1)$ -GFT, while for  $\mathcal{G}_2$  we plot the  $(\mathbf{L}_2, \mathbf{Q}_2)$ -GFT where  $\mathbf{Q}_2$  is chosen according to Theorem 4. As predicted by Proposition 3, the generalized eigenvalues lie in  $[0, 2]$  and  $\lambda_n = 2$  ( $n = 11$ ) for both graphs. The generalized eigenvalue/eigenvector pairs  $(\lambda, \mathbf{u})$  and  $(2 - \lambda, \mathbf{J}\mathbf{u})$  can be easily observed, as predicted by Theorem 4. Note that also for both graphs the generalized eigenvalue  $\lambda = 1$  is simple, thus agreeing with the lower bound  $||\mathcal{A}| - |\mathcal{B}|| = 1$  from Proposition 4. In Figure 6c we plot the  $(\mathbf{L}_2, \mathbf{D}_2)$ -GFT of  $\mathcal{G}_2$ . The graph frequencies belong to the interval  $[0, 2]$ , but they are not symmetric around 1. While both  $(\mathbf{L}_i, \mathbf{D}_i)$ -GFTs are the eigenvectors of the random walk Laplacian, their basis functions are very different, specially at the higher frequencies. Some of the basis functions of  $(\mathbf{L}_2, \mathbf{D}_2)$ -GFTs present some undesirable features such as repeated eigenvalues ( $\lambda_6 = \lambda_7$ ) and localized basis functions  $\mathbf{u}_6, \mathbf{u}_7, \mathbf{u}_9$ . In this example the  $(\mathbf{M}, \mathbf{Q})$ -GFTs that have the spectral folding produce better bases for signal representation.

### B. Vertex domain interpretation

Traditionally, implementations of SGFs using polynomials of the variation operator  $\mathbf{M}$  (i.e., the fundamental matrix of the  $(\mathbf{M}, \mathbf{I})$ -GFT) have been preferred for their efficiency (sparse matrix vector products) and interpretability (localized vertex domain operations). Since  $\mathbf{Q}$  is not diagonal unless the graph is bipartite,  $\mathbf{Z} = \mathbf{Q}^{-1}\mathbf{M}$  can be much denser than  $\mathbf{M}$ , and thus the product  $\mathbf{Z}\mathbf{x}$  may no longer be implemented with localized vertex domain operations.

In this section we show that  $\mathbf{Q}^{-1}$ , and thus the fundamental matrix  $\mathbf{Z}$ , can be approximated by polynomials of sparse matrices. In fact, for certain choices of vertex partitions,  $\mathbf{Z}$  may be approximately sparse and thus the operation  $\mathbf{Z}\mathbf{x}$  is localized in the vertex domain. We show that this product can be described in terms of vertex domain operations involving bipartite and disconnected graphs. The complexity of SGFs as a function of the vertex partition is studied in Section VI.

For simplicity we only consider the combinatorial Laplacian, so that  $\mathbf{M} = \mathbf{L}$ . Given a vertex partition  $\mathcal{A}, \mathcal{B}$ , any graph can be decomposed as the sum of a bipartite graph and a disconnected graph with 2 or more connected components (the adjacency matrix of a disconnected graph is block diagonal if vertices in the same connected component are labeled consecutively). An example is depicted in Figure 2. These graphs obey the following identities

$$\mathbf{L} = \mathbf{L}^{bi} + \mathbf{L}^{bd}, \quad \mathbf{W} = \mathbf{W}^{bi} + \mathbf{W}^{bd}, \quad \mathbf{D} = \mathbf{D}^{bi} + \mathbf{D}^{bd}, \quad (61)$$

where the super indices  $bi$  and  $bd$  refer to bipartite and block diagonal, respectively (see Figure 2). In addition, we have that

$$\mathbf{L}^{bd} = \mathbf{D}^{bd} - \mathbf{W}^{bd}, \quad \mathbf{L}^{bi} = \mathbf{D}^{bi} - \mathbf{W}^{bi}. \quad (62)$$

We have the following factorization for  $\mathbf{Z}$ .

**Proposition 6.** *If  $\mathbf{M} = \mathbf{L}$  and  $(\mathbf{L}, \mathbf{Q})$ -GFT has the spectral folding property, then the fundamental matrix is equal to*

$$\mathbf{Z} = \mathbf{Q}^{-1}\mathbf{L} = \mathbf{I} - \mathbf{P}^{bd}\mathbf{P}^{bi}, \quad (63)$$

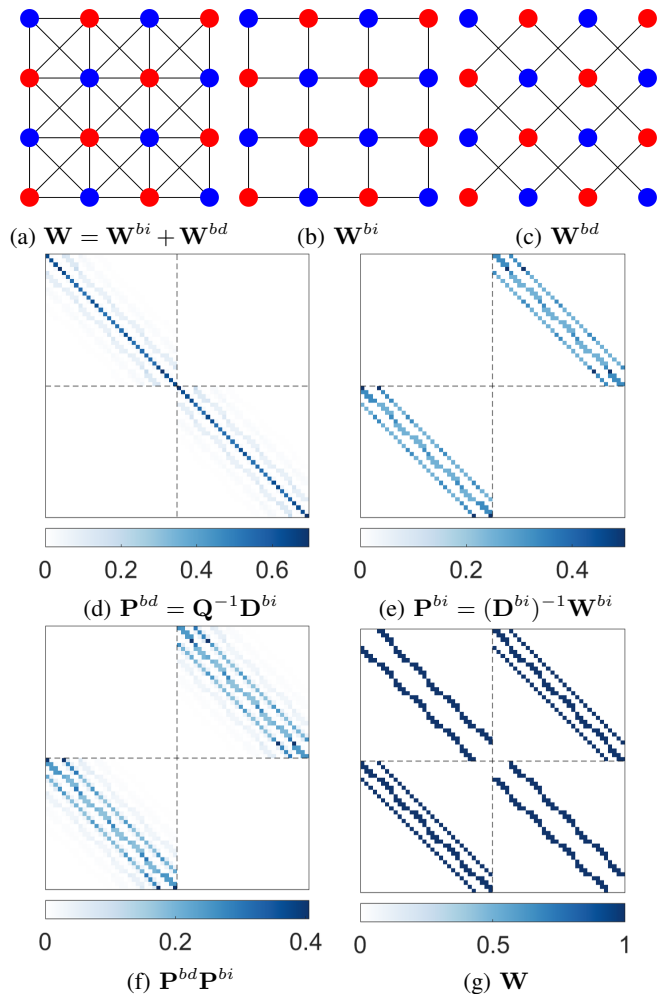


Fig. 7: Decomposition of 8 connected  $4 \times 4$  grid graph (7a) as sum of bipartite (7b) and block diagonal graphs (7c). Graph matrices from Proposition 6 are shown in Figures 7d- 7g.

where  $\mathbf{P}^{bi} = (\mathbf{D}^{bi})^{-1}\mathbf{W}^{bi}$ , and  $\mathbf{P}^{bd} = \mathbf{Q}^{-1}\mathbf{D}^{bi}$ , are both right stochastic non negative matrices, with bipartite and block diagonal structure, respectively.

The proof can be found in Appendix IX-A. The matrix  $\mathbf{P}^{bd}\mathbf{P}^{bi}$  is a two step smoothing operator, since

$$y_i = (\mathbf{P}^{bi}\mathbf{x})_i = \begin{cases} \frac{1}{(\mathbf{D}^{bi})_{ii}} \sum_{j \in \mathcal{B}} w_{ij} x_j & \text{if } i \in \mathcal{A} \\ \frac{1}{(\mathbf{D}^{bi})_{ii}} \sum_{j \in \mathcal{A}} w_{ij} x_j & \text{if } i \in \mathcal{B}. \end{cases} \quad (64)$$

where a smoothed signal is obtained through linear combinations of neighbors on the complement set. Since  $\mathbf{P}^{bd}$  is block diagonal and non negative, the second filtering step is also a low pass filter that only uses connections within  $\mathcal{A}$  or  $\mathcal{B}$ .

As an example we consider the 8-connected grid graph in Figure 7a, commonly used in image processing [50]. The vertex partition (red or blue) can be used to decompose the graph into (i) a bipartite 4-connected grid (Figure 7b), containing all vertical and horizontal connections, and (ii) a block diagonal graph containing the diagonal connections (see Figure 7c). The adjacency matrix of the 8-connected grid is depicted in Figure 7g, where all the edge weights have been set to 1, and the vertices are labeled so that  $\mathcal{A} = \{1, 2, \dots, |\mathcal{A}|\}$ .  $\mathbf{P}^{bd}$

and  $\mathbf{P}^{bi}$  are depicted in Figure 7d and Figure 7e, respectively, and their product is depicted in Figure 7f. While  $\mathbf{P}^{bi}$  and  $\mathbf{W}$  are sparse, the matrices  $\mathbf{P}^{bd}$  and  $\mathbf{P}^{bd}\mathbf{P}^{bi}$  are dense. However, Figure 7d and Figure 7f show that most of the entries of  $\mathbf{P}^{bd}$  and  $\mathbf{P}^{bd}\mathbf{P}^{bi}$  are close to zero. The approximate sparsity of  $\mathbf{Z}$  and  $\mathbf{P}^{bd}\mathbf{P}^{bi}$  can be explained by the following result.

**Proposition 7.** *Let  $\mathbf{L}$  be the combinatorial Laplacian of a connected graph. If  $\mathbf{Q}$  is chosen according to Theorem 4, then*

$$\mathbf{Q}^{-1} = \mathbf{D}^{-\frac{1}{2}} \left( \sum_{k=0}^{\infty} (\mathbf{D}^{-\frac{1}{2}} \mathbf{W}^{bd} \mathbf{D}^{-\frac{1}{2}})^k \right) \mathbf{D}^{-\frac{1}{2}}. \quad (65)$$

*Proof.* Because the graph is connected,  $\mathbf{Q} \succ 0$ . Since  $\mathbf{Q} = \mathbf{D} - \mathbf{W}^{bd}$ , we have that  $\mathbf{I} - \mathbf{D}^{-1/2} \mathbf{W}^{bd} \mathbf{D}^{-1/2} \succ 0$ , which implies that  $\|\mathbf{D}^{-1/2} \mathbf{W}^{bd} \mathbf{D}^{-1/2}\| < 1$ . Then  $(\mathbf{I} - \mathbf{D}^{-1/2} \mathbf{W}^{bd} \mathbf{D}^{-1/2})^{-1} = \sum_{k=0}^{\infty} (\mathbf{D}^{-1/2} \mathbf{W}^{bd} \mathbf{D}^{-1/2})^k$ , and  $\mathbf{Q}^{-1} = \mathbf{D}^{-1/2} (\mathbf{I} - \mathbf{D}^{-1/2} \mathbf{W}^{bd} \mathbf{D}^{-1/2})^{-1} \mathbf{D}^{-1/2}$ .  $\square$

If we only keep the first  $m$  terms in (65), the norm of the remaining terms decays exponentially as  $\mathcal{O}(\|\mathbf{D}^{-1/2} \mathbf{W}^{bd} \mathbf{D}^{-1/2}\|^{m+1})$ . If the vertex partition is designed so that  $\mathbf{W}^{bd}$  is sparse and has small weights, this error decays faster. While in this work we do not approximate  $\mathbf{Q}^{-1}$ , we propose a vertex partitioning algorithm (Section VI) that minimizes the  $\ell_1$  norm of  $\mathbf{D}^{-1/2} \mathbf{W}^{bd} \mathbf{D}^{-1/2}$  that leads to a sparse  $\mathbf{Q}$ , and an approximately sparse fundamental matrix  $\mathbf{Z}$ .

### C. A probabilistic interpretation of GFBs

Our analysis is based on the lazy filter bank from Figure 3. Assume that  $\mathbf{x}$  is a zero mean Gaussian vector with covariance matrix  $\Sigma$ , and select  $\mathbf{M} = \Sigma^{-1}$  as the variation operator. We will show that  $\mathbf{Z}$  given by (34) is the matrix that produces high pass coefficients  $\mathbf{Z}\mathbf{x}$  with the least norm, hence  $\mathbf{Z}$  solves

$$\min_{\mathbf{C}} \mathbb{E}[\|\mathbf{C}\mathbf{x}\|_{\mathbf{I}}^2], \text{ s.t. } \mathbf{C} = \begin{bmatrix} \mathbf{I}_A & \mathbf{C}_{AB} \\ \mathbf{C}_{BA} & \mathbf{I}_B \end{bmatrix}, \quad (66)$$

where  $\mathcal{A}$  and  $\mathcal{B} = \mathcal{V} \setminus \mathcal{A}$  are fixed, and  $\mathbf{C}$  is the high pass filter of the lazy two channel filter bank from Figure 3. Later we study properties of the tree structured iterated lazy filter bank, and provide an alternative probabilistic perspective on its orthogonality. We can reduce (66) to the equivalent problem

$$\begin{aligned} & \min_{\mathbf{C}_{AB}, \mathbf{C}_{BA}} \mathbb{E}[\|\mathbf{x}_A + \mathbf{C}_{AB}\mathbf{x}_B\|_{\mathbf{I}}^2] + \mathbb{E}[\|\mathbf{x}_B + \mathbf{C}_{BA}\mathbf{x}_A\|_{\mathbf{I}}^2] \quad (67) \\ & = \min_{\mathbf{C}_{AB}} \mathbb{E}[\|\mathbf{x}_A + \mathbf{C}_{AB}\mathbf{x}_B\|_{\mathbf{I}}^2] + \min_{\mathbf{C}_{BA}} \mathbb{E}[\|\mathbf{x}_B + \mathbf{C}_{BA}\mathbf{x}_A\|_{\mathbf{I}}^2]. \end{aligned}$$

Minimization of  $\mathbb{E}[\|\mathbf{x}_A + \mathbf{C}_{AB}\mathbf{x}_B\|_{\mathbf{I}}^2]$  corresponds to optimal linear prediction of  $\mathbf{x}_A$  from  $\mathbf{x}_B$ , which fortunately, has a closed form solution for Gaussian distributions.

**Proposition 8.** *Given a vertex partition  $\mathcal{A}, \mathcal{B}$ , if  $\mathbf{M} = \Sigma^{-1}$ , then  $\mathbf{Z} = \mathbf{Q}^{-1}\mathbf{M}$  from (34) is the minimizer of (66), and*

$$\mathbf{Z}\mathbf{x} = \mathbf{x} - \begin{bmatrix} \mathbb{E}[\mathbf{x}_A|\mathbf{x}_B] \\ \mathbb{E}[\mathbf{x}_B|\mathbf{x}_A] \end{bmatrix} = \mathbf{x} - \begin{bmatrix} \Sigma_{AB}\Sigma_{BB}^{-1}\mathbf{x}_B \\ \Sigma_{BA}\Sigma_{AA}^{-1}\mathbf{x}_A \end{bmatrix}. \quad (68)$$

The proof of this result is a direct consequence of

$$\Sigma_{AB}\Sigma_{BB}^{-1} = -\mathbf{M}_{AA}^{-1}\mathbf{M}_{AB}, \Sigma_{BA}\Sigma_{AA}^{-1} = -\mathbf{M}_{BB}^{-1}\mathbf{M}_{BA}, \quad (69)$$

which follows from  $\mathbf{M}\Sigma = \mathbf{I}$ . From the  $(\mathbf{M}, \mathbf{Q})$ -GFT perspective,  $\mathbf{Z}$  is a high pass filter (see Section V-B). Proposition 8 illustrates that the filtering operation  $\mathbf{Z}\mathbf{x}$  is the prediction error of an optimal linear predictor for the Gaussian distribution.

Now we take the lazy filter bank from Figure 3 and form a tree structured filter bank as in Figure 4. Filters at resolution  $\ell$  are given by  $\mathbf{H}_{0,\ell} = \mathbf{I}$ ,  $\mathbf{H}_{1,\ell} = \mathbf{Z}_\ell$ ,  $\mathbf{G}_{0,\ell} = 2\mathbf{I} - \mathbf{Z}_\ell$ , and  $\mathbf{G}_{1,\ell} = \mathbf{I}$ . We will show that Proposition 8 implies that this tree structured filter bank produces sub-bands with uncorrelated coefficients. Assume that the input signal  $\mathbf{x} = \mathbf{a}_L$  is a zero mean Gaussian with covariance  $\Sigma = \mathbf{M}^{-1}$ . Since the low pass channel corresponds to down-sampling  $\mathbf{a}_{\ell+1}$  on the set  $\mathcal{A}_\ell$ , we have that for  $\ell < L$

$$\mathbf{a}_\ell = \mathbf{x}_{\mathcal{A}_\ell}, \quad (70)$$

is a  $|\mathcal{A}_\ell|$ -dimensional zero mean Gaussian vector with covariance matrix  $\Sigma_{\mathcal{A}_\ell, \mathcal{A}_\ell}$ . Therefore, at resolution  $\ell$  we will use the variation operator  $\mathbf{M}_\ell = \Sigma_{\mathcal{A}_\ell, \mathcal{A}_\ell}^{-1}$ , which can be computed using Schur complements [68]

$$\mathbf{M}_{\ell-1} = (\mathbf{M}_\ell)_{\mathcal{A}_\ell \mathcal{A}_\ell} - (\mathbf{M}_\ell)_{\mathcal{A}_\ell \mathcal{B}_\ell} ((\mathbf{M}_\ell)_{\mathcal{B}_\ell \mathcal{B}_\ell})^{-1} (\mathbf{M}_\ell)_{\mathcal{B}_\ell \mathcal{A}_\ell}. \quad (71)$$

The detail coefficients are

$$\mathbf{d}_\ell = \mathbf{x}_{\mathcal{B}_\ell} - \Sigma_{\mathcal{B}_\ell \mathcal{A}_\ell} \Sigma_{\mathcal{A}_\ell \mathcal{A}_\ell}^{-1} \mathbf{x}_{\mathcal{A}_\ell}. \quad (72)$$

The coefficient vector obtained after iterating the filter bank  $L$  times is given by  $\mathbf{c} = [\mathbf{a}_0^\top, \mathbf{d}_0^\top, \dots, \mathbf{d}_{L-1}^\top]^\top = \mathcal{T}_a \mathbf{x}$ . These coefficients are uncorrelated, more precisely:

**Proposition 9.** *The inverse covariance matrix of  $\mathbf{c}$  is equal to*

$$(\mathbb{E}[\mathbf{c}\mathbf{c}^\top])^{-1} = \begin{bmatrix} \mathbf{M}_0 & \mathbf{0} & \dots & \mathbf{0} \\ \mathbf{0} & \mathbf{Q}_{1,0} & \ddots & \mathbf{0} \\ \vdots & \ddots & \ddots & \vdots \\ \mathbf{0} & \mathbf{0} & \mathbf{0} & \mathbf{Q}_{1,L-1} \end{bmatrix}, \quad (73)$$

where  $\mathbf{Q}_{1,\ell}$  is the submatrix given by

$$\mathbf{Q}_{1,\ell} = \mathbf{Q}_{\ell+1}(\mathcal{B}_\ell, \mathcal{B}_\ell). \quad (74)$$

The proof follows from Proposition 8 (see Appendix IX-D).

## VI. VERTEX PARTITIONING

In this section we assume  $\mathbf{M}$  is given, and we wish to optimize  $\mathcal{A}$  and  $\mathcal{B} = \mathcal{V} \setminus \mathcal{A}$ , as a function of  $\mathbf{M}$ . We start by formulating this problem as an optimization of the condition number of  $\mathbf{Q}$ . We provide some theoretical justifications for this choice of objective based on complexity and stability of GFBs. We end the section with our proposed solution.

### A. Problem formulation

$\mathbf{J}$  defined in (23) completely characterizes the vertex partition since  $\mathbf{J}_{ii} = 1$  if  $i \in \mathcal{A}$ , and  $\mathbf{J}_{ii} = -1$  if  $i \in \mathcal{B}$ . Consequently, we will use a vector  $\mathbf{f}$  containing the diagonal terms of  $\mathbf{J}$  as an optimization variable. We propose to minimize

$\kappa(\mathbf{Q}) = \|\mathbf{Q}\| \|\mathbf{Q}^{-1}\|$ , the condition number of  $\mathbf{Q}$ , subject to spectral folding and balanced partition constraints, namely,

$$\min_{\mathbf{f}: \mathbf{f}_i^2=1} \kappa(\mathbf{Q}) \quad \text{s.t. } \mathbf{Q} = \frac{1}{2}(\mathbf{M} + \text{diag}(\mathbf{f})\mathbf{M}\text{diag}(\mathbf{f})) \quad (75)$$

$$\left| \sum_{i \in \mathcal{V}} \mathbf{f}_i \right| \leq 1.$$

The constraint  $\mathbf{f}_i^2 = 1$  ensures that the vector  $\mathbf{f}$  has entries equal to 1 or  $-1$ . The downsampling sets are recovered as  $\mathcal{A} = \{i : \mathbf{f}_i > 0\}$ , and  $\mathcal{B} = \mathcal{A}^c$ . To ensure the  $(\mathbf{M}, \mathbf{Q})$ -GFT has the spectral folding property we incorporate the constraint  $\mathbf{Q} = \frac{1}{2}(\mathbf{M} + \text{diag}(\mathbf{f})\mathbf{M}\text{diag}(\mathbf{f}))$ . When there is an even number of nodes, the constraint  $|\sum_{i \in \mathcal{V}} \mathbf{f}_i| \leq 1$  becomes  $\sum_{i \in \mathcal{V}} \mathbf{f}_i = 0$  so that  $|\mathcal{A}| = |\mathcal{B}|$ . When the number of nodes is odd, the constraint  $|\sum_{i \in \mathcal{V}} \mathbf{f}_i| \leq 1$  becomes  $|\sum_{i \in \mathcal{V}} \mathbf{f}_i| = 1$ , so that  $||\mathcal{A}| - |\mathcal{B}|| = 1$ . These constraints guarantee a balanced partition, which is a necessary condition for good frequency selectivity (see Section V-A for more details).

### B. Justification for condition number minimization

The reason for seeking vertex partitions so that the  $\mathbf{Q}$  has a small condition number is due to numerical stability and complexity of GFBs. For large graphs, performing eigendecomposition to implement a SGF is infeasible due to high computational complexity, thus polynomial graph filters are used instead. For BFBs, a polynomial graph filter of degree  $d$  can be implemented by sparse matrix vector products (of the normalized Laplacian) with complexity  $\mathcal{O}(d|\mathcal{E}|)$  [10], [12]. For arbitrary graphs, polynomials of  $\mathbf{Z}$  require the computation of products of the form  $\mathbf{Z}\mathbf{x}$ . However, although  $\mathbf{M}$  may be sparse, the fundamental matrix  $\mathbf{Z} = \mathbf{Q}^{-1}\mathbf{M}$  is not. Hence, a naive implementation of the product  $\mathbf{Z}\mathbf{x}$  has complexity  $\mathcal{O}(n^2)$ , while direct computation of  $\mathbf{Z} = \mathbf{Q}^{-1}\mathbf{M}$  has complexity  $\mathcal{O}(n^3)$  due to matrix inversion. A more efficient approach is to decompose the product  $\mathbf{y} = \mathbf{Z}\mathbf{x}$  into: 1) computing a sparse matrix vector product  $\mathbf{w} = \mathbf{M}\mathbf{x}$ , and 2) solving a system of equations  $\mathbf{Q}\mathbf{y} = \mathbf{w}$ . The second step is the computation bottleneck, since it requires solving a linear system.

Large scale positive semi-definite linear system are solved by iterative methods such as the Conjugate Gradient (CG), whose complexity per iteration is that of a sparse matrix vector products with  $\mathbf{Q}$ . The condition number of  $\mathbf{Q}$  is directly responsible for: 1) the convergence rate of CG algorithms (and thus the total number of iterations), and 2) stability to perturbations of the system  $\mathbf{Q}\mathbf{y} = \mathbf{w}$ . From a computational perspective, the best case scenario occurs when  $\mathbf{Q}$  is sparse and has a small condition number. In practice this is attained when  $\mathbf{Q}$  is diagonal, and the graph is bipartite, as will be shown in the next subsection.

### C. Approximate solution for generalized Laplacians

Because of the non convex constraint  $\mathbf{f}_i^2 = 1$ , (75) is a non convex minimization problem. In this section we obtain an upper bound for  $\kappa(\mathbf{Q})$ , which allows us to pose an alternative, more tractable optimization problem. For the rest of this section we assume that  $\mathbf{M}$  is a positive semi definite

generalized graph Laplacian, that is,  $\mathbf{M} = \mathbf{V} - \mathbf{W}$ , where  $\mathbf{V}$  is a diagonal matrix with positive entries and  $\mathbf{W}$  is a non negative matrix with zero diagonal. Since  $\mathbf{Q}$  is given by Theorem 4, we have that  $\mathbf{Q} = \mathbf{V} - \mathbf{W}^{bd} \succ 0$ , where  $\mathbf{W}^{bd} = (1/2)(\mathbf{W} + \text{diag}(\mathbf{f})\mathbf{W}\text{diag}(\mathbf{f}))$  is the block diagonal part of  $\mathbf{W}$ . We can bound  $\kappa(\mathbf{Q})$  with

$$\kappa(\mathbf{Q}) \leq \kappa(\mathbf{V})(1 + \rho(\mathcal{A}))/ (1 - \rho(\mathcal{A})), \quad (76)$$

where  $\kappa(\mathbf{V})$  is the condition number of  $\mathbf{V}$ , and  $\rho(\mathcal{A}) = \|\mathbf{V}^{-1/2}\mathbf{W}^{bd}\mathbf{V}^{-1/2}\|$ . A derivation of this bound is given in Appendix IX-E. When the graph is bipartite,  $\mathbf{f}$  can be chosen so that  $\mathbf{Q}$  is diagonal resulting in  $\rho(\mathcal{A}) = 0$ , making the bound tight. Since the right side of (76) is decreasing with  $\rho(\mathcal{A})$ , we can minimize  $\rho(\mathcal{A})$  as a function of the vertex partition. As a simplification, we use the sequence of bounds for the operator norm of a matrix,  $\|\mathbf{A}\| \leq \|\mathbf{A}\|_F \leq \|\mathbf{A}\|_1 = \sum_{i,j} |a_{ij}|$ , which results in  $\rho(\mathcal{A}) \leq \sum_{i,j} (1 + \mathbf{f}_i \mathbf{f}_j) w_{ij} / \sqrt{v_i v_j}$ . We propose solving instead:

$$\min_{\mathbf{f}: \mathbf{f}_i^2=1} \sum_{i,j} (1 + \mathbf{f}_i \mathbf{f}_j) \tilde{w}_{ij} \quad \text{s.t. } \left| \sum_{i \in \mathcal{V}} \mathbf{f}_i \right| \leq 1 \quad (77)$$

where  $\tilde{w}_{ij}$  is the  $ij$  entry of  $\tilde{\mathbf{W}} = \mathbf{V}^{-1/2}\mathbf{W}\mathbf{V}^{-1/2}$ . Using the identity  $\sum_{i,j} \mathbf{f}_i \mathbf{f}_j \tilde{w}_{ij} = \mathbf{f}^\top \tilde{\mathbf{W}} \mathbf{f} = \sum_{i,j} \tilde{w}_{ij} - \mathbf{f}^\top \tilde{\mathbf{L}} \mathbf{f}$ , we have that (77) is equivalent to

$$\max_{\mathbf{f}: \mathbf{f}_i^2=1} \mathbf{f}^\top \tilde{\mathbf{L}} \mathbf{f} \quad \text{s.t. } \left| \sum_{i \in \mathcal{V}} \mathbf{f}_i \right| \leq 1, \quad (78)$$

where  $\tilde{\mathbf{D}} = \text{diag}(\tilde{\mathbf{W}}\mathbf{1})$ , and  $\tilde{\mathbf{L}} = \tilde{\mathbf{D}} - \tilde{\mathbf{W}}$ . (78) is an instance of weighted maximum cut (WMC) [71], with an additional balanced partition constraint. It is well known that WMC is NP hard, thus we consider a spectral partitioning approximation [9], [72], that computes  $\tilde{\mathbf{u}}_n = \arg \max_{\|\mathbf{u}\|=1} \mathbf{u}^\top \tilde{\mathbf{L}} \mathbf{u}$ , and sets  $\mathbf{f} = \text{sign}(\tilde{\mathbf{u}}_n - \tau \mathbf{1})$ , and  $\mathcal{A} = \{i \in \mathcal{V} : \mathbf{f}_i = 1\}$ . The parameter  $\tau \in \mathbb{R}$  can be tuned to ensure  $|\sum_{i \in \mathcal{V}} \mathbf{f}_i| \leq 1$ .

### D. Minnesota graph example

We implement the proposed max-cut vertex partitioning algorithm and a random partitioning algorithm that assigns nodes to  $\mathcal{A}$  with probability 1/2. We consider the Minnesota road graph [69], which has  $n = 2640$  nodes and  $s = 3302$  edges with unit weights. Its adjacency matrix  $\mathbf{W}$  is depicted in Figure 8a. We use the combinatorial Laplacian  $\mathbf{L}$  as variation operator. In Figure 8 we display the sparsity patterns of  $\mathbf{W}^{bd} = \mathbf{D} - \mathbf{Q} = (1/2)(\mathbf{W} + \text{diag}(\mathbf{f})\mathbf{W}\text{diag}(\mathbf{f}))$ , where  $\mathbf{f}$  has been obtained via the proposed max-cut sampling (Figure 8b) and via random partitioning (Figure 8c). Random vertex partition produces a less sparse matrix  $\mathbf{Q}$ , which retains 49.6% of the edges from  $\mathbf{W}$ . In contrast, the proposed max-cut vertex partitioning, produces a matrix  $\mathbf{Q}$  which only has 14.56% of the edges of  $\mathbf{W}$ , and is much closer to  $\mathbf{D}$ . We also compare the condition numbers of  $\mathbf{Q}$  as a function of the vertex partition. We generate 1000 realizations of random partitions, and display the distribution of  $\kappa(\mathbf{Q})/\kappa(\mathbf{D})$  in Figure 9. The proposed max-cut partition achieves  $\kappa(\mathbf{Q})/\kappa(\mathbf{D}) = 1.863$ , and our simulation shows that the normalized condition number is always greater than

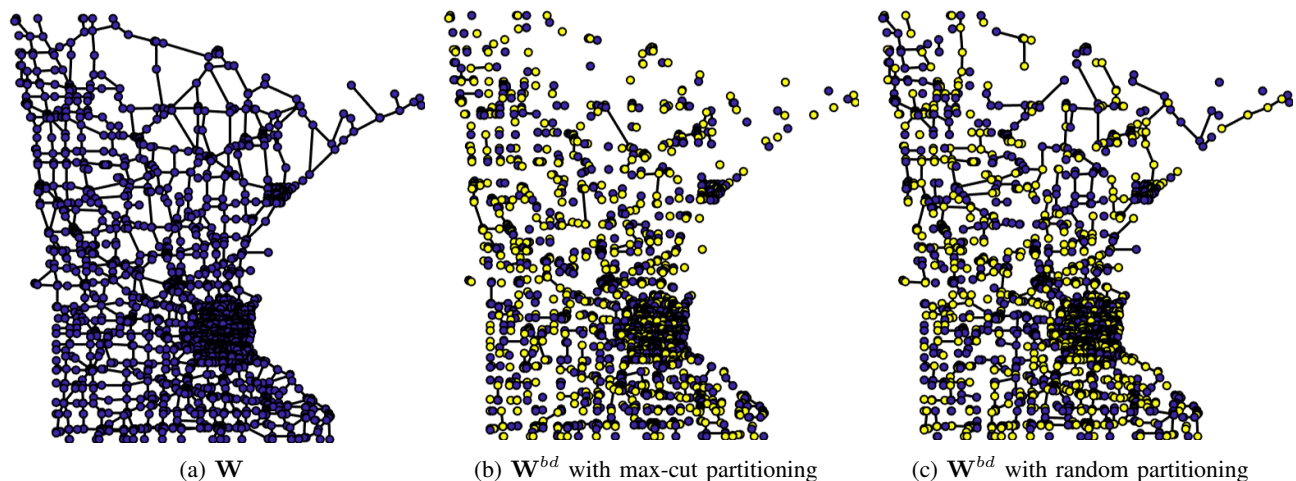


Fig. 8: Comparison of matrices  $\mathbf{W}^{bd} = \frac{1}{2}(\mathbf{W} + \text{diag}(\mathbf{f})\mathbf{W}\text{diag}(\mathbf{f}))$  using different vertex partitioning algorithms for the Minnesota graph [69]. Vertex partitions are marked by blue/yellow circles. Figures were generated using the toolbox [70].

1.863 for the the random partitions. Because the Minnesota graph is very sparse ( $s = 3302 \approx 1.25n$ ), the sub-graph associated to  $\mathbf{P}^{bd}$  (and  $\mathbf{Q}$ ) have many more than 2 connected components, resulting in both  $\mathbf{Z}$  and  $\mathbf{Q}^{-1}$  also being exactly sparse. When using max-cut partitioning  $\mathbf{Z}$  has  $1.2806s$  non-zero off diagonal entries, but when random partitioning is used the number of non-zero off diagonal entries in  $\mathbf{Z}$  ranges from  $2.7733s$  to  $4.4170s$ , with average  $3.3559s$ . In the next section, we show that this algorithm can be efficiently implemented for large graphs (since it only requires computing an eigenvector), while improving the signal representation.

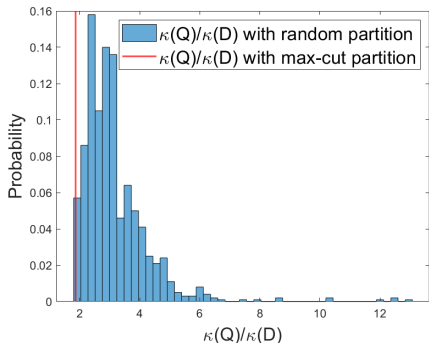


Fig. 9: Distribution of the normalized condition number of  $\mathbf{Q}$  when using random vertex partitioning.

## VII. EXPERIMENTS ON 3D POINT CLOUDS

In this section we present numerical results showing that: 1) GFB can be implemented efficiently on graphs with hundreds of thousands of nodes, 2) the basis functions of GFBs are localized in the vertex domain and 3) for point clouds, GFBs with optimized vertex partitions can provide better signal representations than BFBs.

### A. Vertex domain localization

We start by visualizing the vertex domain behavior of the GFB basis functions, i.e., the columns of the synthesis operator

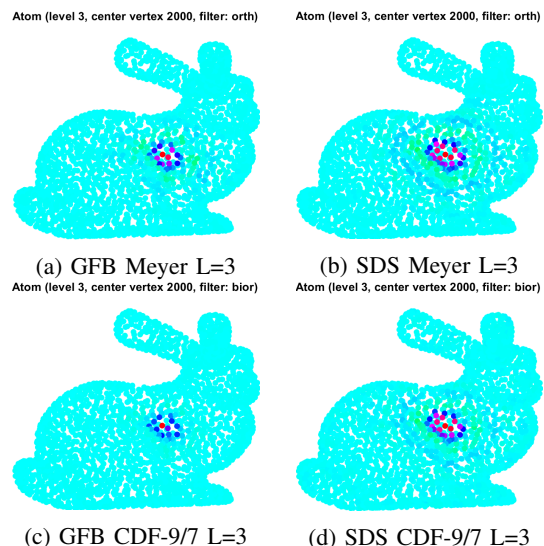


Fig. 10: Low frequency atoms on Bunny point cloud centered at node 2000. (left) Proposed generalized filter banks (GFB), and (right) filter banks based on spectral domain sampling (SDS).

$\mathcal{T}_s$  of a tree structured filter bank (see Section IV-G and Figure 4). We compare them to those of spectral domain sampling (SDS) filter banks [47], which are close to the proposed GFB in terms of graph properties (see Table I). We show that although  $\mathbf{Z}$  is (numerically) dense, for point clouds,  $\mathbf{Z}$  is approximately sparse and polynomial filters of  $\mathbf{Z}$  are localized in the vertex domain.

Since SDS filter banks require full eigendecomposition, for complexity reasons we use a small *Bunny* point cloud, which has  $n = 2503$  nodes. For both filter banks we fix the number of levels to  $L = 3$  and consider two designs: biorthogonal CDF-9/7 filters, and orthogonal Meyer filters. Note that these filters are exactly those developed for traditional 1D wavelets. For graph construction, we use nonnegative kernel regression (NNK) [73] initialized with k-nearest-neighbors (KNN) using

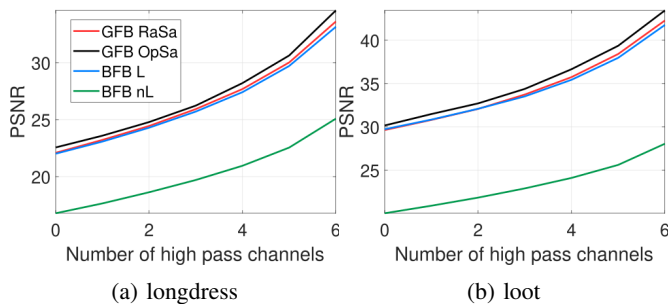


Fig. 11: 3D point cloud attribute approximation. GFBs with random partitioning (GFB RaSa) and max-cut partitioning from Section VI (GFB OpSa). BFBs using random partitioning with the combinatorial Laplacian (BFB L), and the normalized Laplacian (BFB nL).

$K = 20$  and inverse distance as edge weights. For GFBs, we use the spectral partitioning algorithm from Section VI. Figure 10 displays low frequency basis functions, centered at a single node. For visualization purposes, we normalize the basis functions, so their entries have magnitude at most 1. For both filter designs, the basis functions of the GFBs are more localized than their SDS counterparts. The GFB with CDF-9/7 filters is implemented using polynomials of  $\mathbf{Z}$ , thus producing the most localized basis functions.

### B. Representation of 3D point cloud attributes

3D point clouds consist of list of point coordinates  $\mathbf{V} = [\mathbf{v}_i] \in \mathbb{R}^{n \times 3}$ , and color attributes  $\mathbf{A} \in \mathbb{R}^{n \times 3}$ . A graph is constructed where each point is assigned to a node and the edge weight between nodes  $i$  and  $j$  is  $w_{ij} = 1/\|\mathbf{v}_i - \mathbf{v}_j\|$ . A sparse edge set is obtained using the KNN and NNK [73] graph construction algorithms. We consider the first frame of the *loot* and *longdress* sequences of the 8iVFBv2 dataset [32], which have  $n = 784,142$  and  $n = 765,821$  points respectively. We implement the tree structured GFB of Figure 4 with  $L = 7$  levels, using biorthogonal analysis filters  $h_0(\lambda) = \frac{1}{2a_0}(2 - \lambda)(1 + \lambda)$ , and  $h_1(\lambda) = a_0\lambda$ , with gain  $a_0 = 0.735$ , and synthesis filters computed with (28).

We apply the GFB to each column of the color matrix  $\mathbf{A}$  independently, and obtain the approximation by only keeping the low-pass coefficients  $\mathbf{a}_0$  and a subset of the high-pass coefficients  $\mathbf{d}_i$  for  $0 \leq i \leq m - 1$ , with  $m \in \{1, \dots, L\}$ , and zeroing out the rest. For each filter bank, we tested various graph constructions and chose the one giving the best performance. We tested KNN graphs with  $K \in \{5, 10, 15, 20\}$  and NNK graphs initialized with KNN using  $K = 20$ . To construct bipartite graphs, we take a KNN or NNK graph, a random vertex partition  $\mathcal{A}, \mathcal{B}$ , and use the subgraph consisting of only the edges from  $\mathcal{A}$  to  $\mathcal{B}$ . For GFBs, the best results (higher PSNR) are obtained with NNK graphs, while for BFB the best results are obtained with KNN graphs. Figure 11 shows the PSNR between the color signal and its approximation as a function of the number of high pass channels ( $m$ ). As expected, the BFB with the normalized Laplacian has the worst performance, which can be attributed to the non constant DC signal [11], [28]. By using the BFB with

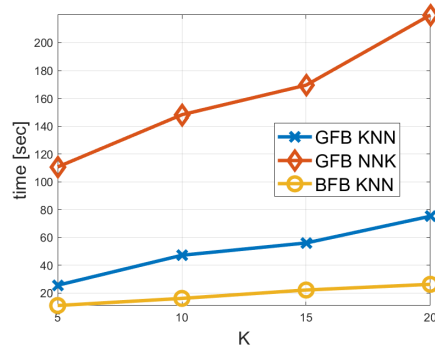


Fig. 12: Run time of BFBs implemented with random vertex partitioning and KNN graphs, and GFBs implemented with max-cut vertex partitioning on KNN and NNK graphs. The first 20 frames of the “longdress” sequence of 3D point clouds are considered.

the  $(\mathbf{L}, \mathbf{D})$ -GFT, which results in the random walk Laplacian, we recover the zeroDC filter bank from [11], which has a much improved performance, consistent with previous studies [11], [28]. The proposed GFB with random sampling always outperforms the best BFB, although by a small margin. When using optimal sampling with GFBs, performance is again improved consistently across datasets<sup>3</sup>.

### C. Complexity

We compute the run time of the tree structured analysis and synthesis filter banks with  $L = 7$  levels using the biorthogonal filters from the previous section, applied to the first 20 frames of the “longdress” sequence. These point clouds have an average of approximately 795,000 points per frame. We compare BFBs constructed with KNN graphs and random balanced partitioning (BFB KNN), GFB constructed with KNN graphs and max-cut based vertex partitioning (GFB KNN), and GFB constructed with NNK graphs and max-cut based vertex partitioning (GFB NNK). NNK graphs are initialized with KNN graphs with varying parameters  $K$ . The complexity of our implementation is dominated by graph construction (KNN and NNK), vertex partitioning, and solving the sparse linear system of the form  $\mathbf{Q}\mathbf{z} = \mathbf{u}$ . The complexity of each of these components is proportional to the graph sparsity, and the parameter  $K$  in KNN. In Figure 12 we plot the average run time over 20 trials as a function of  $K$ . Note that  $K$  serves as a proxy for graph sparsity since the number of edges in a KNN and NNK graphs is  $\mathcal{O}(nK)$ . The figure shows that our implementations of GFB has a run time higher than their BFB counterparts, but still scales approximately linearly with  $K$ .

## VIII. CONCLUSION

This paper proposed two-channel filter banks on arbitrary graphs with positive semi definite variation operators  $\mathbf{M}$  and arbitrary vertex partitions  $\mathcal{A}, \mathcal{B}$  for downsampling. Because of the spectral folding property, previous designs were only

<sup>3</sup>The superiority of GFBs is consistent for other frames, and other sequences of the 8i dataset. Those results are omitted due to space.

valid for the normalized Laplacian of bipartite graphs. Our main contribution is showing that the spectral folding property is satisfied by the generalized eigenvalues and eigenvectors of arbitrary graphs, if the inner product matrix is properly chosen. Based on this, we proposed generalized filter banks (GFB) implemented with spectral graph filters of the generalized eigenvectors. We also studied other theoretical aspects of GFBs including: properties of the generalized eigenvalues, vertex domain localization and probabilistic interpretations. We showed that even though GFBs can use arbitrary vertex partitions for downsampling, partitions that have a large cut (the sum of edge weights from  $\mathcal{A}$  to  $\mathcal{B}$  is large) lead to computationally efficient and stable implementations. Our numerical results show that indeed, GFBs have localized basis functions and they can be efficiently implemented on large graphs with hundreds of thousands of nodes, while outperforming bipartite filter banks on a signal representation tasks. Some important directions for future work include:

*Tree structured filter banks:* We constructed tree structured GFBs by concatenating two channel GFBs. There is ample room for study of properties of these tree structured filter banks from both probabilistic perspectives (beyond the lazy filter bank case), and the design of variation and downsampling operators. In the supplementary material we obtain frame bounds that reveal some of these multi resolution dependencies.

*Vertex partitioning:* Better vertex partitions could be obtained using different approximations to (75) or other objective functions, e.g., by using probabilistic models as in Section V, or techniques from the graph signal sampling literature [74].

## REFERENCES

- [1] A. Ortega, P. Frossard, J. Kovačević, J. M. Moura, and P. Vandergheynst, "Graph signal processing: Overview, challenges, and applications," *Proceedings of the IEEE*, vol. 106, no. 5, pp. 808–828, 2018.
- [2] D. I. Shuman, S. K. Narang, P. Frossard, A. Ortega, and P. Vandergheynst, "The emerging field of signal processing on graphs: Extending high-dimensional data analysis to networks and other irregular domains," *IEEE signal processing magazine*, vol. 30, no. 3, pp. 83–98, 2013.
- [3] A. Sandryhaila and J. M. Moura, "Discrete signal processing on graphs," *IEEE transactions on signal processing*, vol. 61, no. 7, pp. 1644–1656, 2013.
- [4] A. Ortega, *Introduction to Graph Signal Processing*. Cambridge University Press, 2022.
- [5] M. Vetterli and J. Kovacevic, *Wavelets and subband coding*. Prentice-hall, 1995.
- [6] I. Daubechies, *Ten lectures on wavelets*. Siam, 1992, vol. 61.
- [7] P. P. Vaidyanathan, *Multirate systems and filter banks*. Pearson Education India, 2006.
- [8] S. Mallat, *A wavelet tour of signal processing*. Elsevier, 1999.
- [9] D. I. Shuman, "Localized spectral graph filter frames: A unifying framework, survey of design considerations, and numerical comparison," *IEEE Signal Processing Magazine*, vol. 37, no. 6, pp. 43–63, 2020.
- [10] S. K. Narang and A. Ortega, "Perfect reconstruction two-channel wavelet filter banks for graph structured data," *IEEE Transactions on Signal Processing*, vol. 60, no. 6, pp. 2786–2799, 2012.
- [11] —, "Compact support biorthogonal wavelet filterbanks for arbitrary undirected graphs," *IEEE transactions on signal processing*, vol. 61, no. 19, pp. 4673–4685, 2013.
- [12] A. Sakiyama, K. Watanabe, and Y. Tanaka, "Spectral graph wavelets and filter banks with low approximation error," *IEEE Transactions on Signal and Information Processing over Networks*, vol. 2, no. 3, pp. 230–245, 2016.
- [13] D. B. Tay and J. Zhang, "Techniques for constructing biorthogonal bipartite graph filter banks," *IEEE Transactions on Signal Processing*, vol. 63, no. 21, pp. 5772–5783, 2015.
- [14] H. Q. Nguyen, P. A. Chou, and Y. Chen, "Compression of human body sequences using graph wavelet filter banks," in *2014 IEEE International Conference on Acoustics, Speech and Signal Processing (ICASSP)*. IEEE, 2014, pp. 6152–6156.
- [15] A. Anis, P. A. Chou, and A. Ortega, "Compression of dynamic 3d point clouds using subdivisional meshes and graph wavelet transforms," in *2016 IEEE International Conference on Acoustics, Speech and Signal Processing (ICASSP)*. IEEE, 2016, pp. 6360–6364.
- [16] J. Zeng, G. Cheung, Y.-H. Chao, I. Blanes, J. Serra-Sagrìstà, and A. Ortega, "Hyperspectral image coding using graph wavelets," in *2017 IEEE Intl. Conf. on Image Proc. (ICIP)*. IEEE, 2017, pp. 1672–1676.
- [17] D. E. O. Tzamarías, K. Chow, I. Blanes, and J. Serra-Sagrìstà, "Compression of hyperspectral scenes through integer-to-integer spectral graph transforms," *Remote Sensing*, vol. 11, no. 19, p. 2290, 2019.
- [18] Y. Iizuka and Y. Tanaka, "Depth map denoising using collaborative graph wavelet shrinkage on connected image patches," in *2014 IEEE Intl. Conf. on Image Proc. (ICIP)*. IEEE, 2014, pp. 828–832.
- [19] M. Levorato, S. Narang, U. Mitra, and A. Ortega, "Reduced dimension policy iteration for wireless network control via multiscale analysis," in *2012 IEEE Global Communications Conference (GLOBECOM)*. IEEE, 2012, pp. 3886–3892.
- [20] V. K. Sharma, D. K. Srivastava, and P. Mathur, "Efficient image steganography using graph signal processing," *IET Image Processing*, vol. 12, no. 6, pp. 1065–1071, 2018.
- [21] Y.-l. Qiao, Y. Zhao, and X.-y. Men, "Target recognition in sar images via graph wavelet transform and 2DPCA," in *Proceedings of the 2nd Intl. Conf. on Image and Graphics Processing*, 2019, pp. 3–7.
- [22] D. B. Tay and A. Ortega, "Bipartite graph filter banks: Polyphase analysis and generalization," *IEEE Transactions on Signal Processing*, vol. 65, no. 18, pp. 4833–4846, 2017.
- [23] S. K. Narang and A. Ortega, "Local two-channel critically sampled filter-banks on graphs," in *2010 IEEE Intl. Conf. on Image Proc.* IEEE, 2010, pp. 333–336.
- [24] J. Zeng, G. Cheung, and A. Ortega, "Bipartite approximation for graph wavelet signal decomposition," *IEEE Transactions on Signal Processing*, vol. 65, no. 20, pp. 5466–5480, 2017.
- [25] A. Jiang, J. Wan, Y. Tang, B. Ni, and Y. Zhu, "Admm-based bipartite graph approximation," in *ICASSP 2019-2019 IEEE International Conference on Acoustics, Speech and Signal Processing (ICASSP)*. IEEE, 2019, pp. 5421–5425.
- [26] E. Pavez, H. E. Egilmez, and A. Ortega, "Learning graphs with monotone topology properties and multiple connected components," *IEEE Transactions on Signal Processing*, vol. 66, no. 9, pp. 2399–2413, 2018.
- [27] S. Kumar, J. Ying, J. d. M. Cardoso, and D. P. Palomar, "A unified framework for structured graph learning via spectral constraints," *Journal of Machine Learning Research*, vol. 21, no. 22, pp. 1–60, 2020.
- [28] D. E. Tzamarías, E. Pavez, B. Girault, A. Ortega, I. Blanes, and J. Serra-Sagrìstà, "Orthogonality and zero dc tradeoffs in biorthogonal graph filterbanks," in *ICASSP 2021-2021 IEEE International Conference on Acoustics, Speech and Signal Processing (ICASSP)*. IEEE, 2021, pp. 5509–5513.
- [29] B. Girault, A. Ortega, and S. S. Narayanan, "Irregularity-aware graph fourier transforms," *IEEE Transactions on Signal Processing*, vol. 66, no. 21, pp. 5746–5761, 2018.
- [30] D. S. Taubman and M. W. Marcellin, *JPEG2000 - image compression fundamentals, standards and practice*. Kluwer, 2002.
- [31] K.-S. Lu and A. Ortega, "Fast graph fourier transforms based on graph symmetry and bipartition," *IEEE Transactions on Signal Processing*, vol. 67, no. 18, pp. 4855–4869, 2019.
- [32] E. d'Eon, B. Harrison, T. Myers, and P. A. Chou, "8i voxelized full bodies—a voxelized point cloud dataset," *ISO/IEC JTC1/SC29 Joint WG11/WG1 (MPEG/JPEG) input document WG11M40059/WG11M74006*, 2017.
- [33] D. A. Spielman and N. Srivastava, "Graph sparsification by effective resistances," *SIAM Journal on Computing*, vol. 40, no. 6, pp. 1913–1926, 2011.
- [34] M. Hein, J.-Y. Audibert, and U. v. Luxburg, "Graph laplacians and their convergence on random neighborhood graphs," *Journal of Machine Learning Research*, vol. 8, no. Jun, pp. 1325–1368, 2007.
- [35] P. A. Chou, M. Koroteev, and M. Krivokuća, "A volumetric approach to point cloud compression—part i: Attribute compression," *IEEE Transactions on Image Processing*, vol. 29, pp. 2203–2216, 2019.

- [36] M. Krivokuća, P. A. Chou, and M. Koroteev, "A volumetric approach to point cloud compression—part ii: Geometry compression," *IEEE Transactions on Image Processing*, vol. 29, pp. 2217–2229, 2019.
- [37] B. Girault, A. Ortega, and S. S. Narayanan, "Graph vertex sampling with arbitrary graph signal hilbert spaces," in *2020 IEEE International Conference on Acoustics, Speech and Signal Processing (ICASSP)*. IEEE, 2020, pp. 5670–5674.
- [38] K.-S. Lu, A. Ortega, D. Mukherjee, and Y. Chen, "Perceptually inspired weighted mse optimization using irregularity-aware graph fourier transform," in *2020 IEEE Intl. Conf. on Image Proc. (ICIP)*. IEEE, 2020, pp. 3384–3388.
- [39] F. R. Chung and F. C. Graham, *Spectral graph theory*. American Mathematical Soc., 1997, no. 92.
- [40] E. Pavez, B. Girault, A. Ortega, and P. A. Chou, "Spectral folding and two-channel filter-banks on arbitrary graphs," in *2021 IEEE International Conference on Acoustics, Speech, and Signal Processing (ICASSP)*. IEEE, 2021.
- [41] O. Teke and P. P. Vaidyanathan, "Extending classical multirate signal processing theory to graphs—part i: Fundamentals," *IEEE Transactions on Signal Processing*, vol. 65, no. 2, pp. 409–422, 2016.
- [42] —, "Extending classical multirate signal processing theory to graphs—part ii: M-channel filter banks," *IEEE Transactions on Signal Processing*, vol. 65, no. 2, pp. 423–437, 2016.
- [43] A. Sakiyama and Y. Tanaka, "Oversampled graph laplacian matrix for graph filter banks," *IEEE Transactions on Signal Processing*, vol. 62, no. 24, pp. 6425–6437, 2014.
- [44] D. I. Shuman, M. J. Faraji, and P. Vandergheynst, "A multiscale pyramid transform for graph signals," *IEEE Transactions on Signal Processing*, vol. 64, no. 8, pp. 2119–2134, 2015.
- [45] S. Chen, R. Varma, A. Sandryhaila, and J. Kovačević, "Discrete signal processing on graphs: Sampling theory," *IEEE transactions on signal processing*, vol. 63, no. 24, pp. 6510–6523, 2015.
- [46] S. Li, Y. Jin, and D. I. Shuman, "Scalable  $m$ -channel critically sampled filter banks for graph signals," *IEEE Transactions on Signal Processing*, vol. 67, no. 15, pp. 3954–3969, 2019.
- [47] A. Sakiyama, K. Watanabe, Y. Tanaka, and A. Ortega, "Two-channel critically sampled graph filter banks with spectral domain sampling," *IEEE Transactions on Signal Processing*, vol. 67, no. 6, pp. 1447–1460, 2019.
- [48] M. S. Kotzagiannidis and P. L. Dragotti, "Splines and wavelets on circulant graphs," *Applied and Computational Harmonic Analysis*, vol. 47, no. 2, pp. 481–515, 2019.
- [49] V. N. Ekambaram, G. C. Fanti, B. Ayazifar, and K. Ramchandran, "Spline-like wavelet filterbanks for multiresolution analysis of graph-structured data," *IEEE Transactions on Signal and Information Processing over Networks*, vol. 1, no. 4, pp. 268–278, 2015.
- [50] G. Cheung, E. Magli, Y. Tanaka, and M. K. Ng, "Graph spectral image processing," *Proceedings of the IEEE*, vol. 106, no. 5, pp. 907–930, 2018.
- [51] J.-Y. Kao, A. Ortega, and S. S. Narayanan, "Graph-based approach for motion capture data representation and analysis," in *2014 IEEE Intl. Conf. on Image Proc. (ICIP)*. IEEE, 2014, pp. 2061–2065.
- [52] S. K. Narang, Y. H. Chao, and A. Ortega, "Graph-wavelet filterbanks for edge-aware image processing," in *2012 IEEE Statistical Signal Processing Workshop (SSP)*. IEEE, 2012, pp. 141–144.
- [53] K.-S. Lu, E. Pavez, and A. Ortega, "On learning laplacians of tree structured graphs," in *2018 IEEE Data Science Workshop (DSW)*. IEEE, 2018, pp. 205–209.
- [54] A. Anis and A. Ortega, "Critical sampling for wavelet filterbanks on arbitrary graphs," in *2017 IEEE International Conference on Acoustics, Speech and Signal Processing (ICASSP)*. IEEE, 2017, pp. 3889–3893.
- [55] M. Crovella and E. Kolaczyk, "Graph wavelets for spatial traffic analysis," in *IEEE INFOCOM 2003. Twenty-second Annual Joint Conference of the IEEE Computer and Communications Societies (IEEE Cat. No. 03CH37428)*, vol. 3. IEEE, 2003, pp. 1848–1857.
- [56] R. R. Coifman and M. Maggioni, "Diffusion wavelets," *Applied and Computational Harmonic Analysis*, vol. 21, no. 1, pp. 53–94, 2006.
- [57] D. K. Hammond, P. Vandergheynst, and R. Gribonval, "Wavelets on graphs via spectral graph theory," *Applied and Computational Harmonic Analysis*, vol. 30, no. 2, pp. 129–150, 2011.
- [58] A. Cloninger, H. Li, and N. Saito, "Natural graph wavelet packet dictionaries," *Journal of Fourier Analysis and Applications*, vol. 27, no. 3, pp. 1–33, 2021.
- [59] X. Dong, D. Thanou, M. Rabbat, and P. Frossard, "Learning graphs from data: A signal representation perspective," *IEEE Signal Processing Magazine*, vol. 36, no. 3, pp. 44–63, 2019.
- [60] G. Mateos, S. Segarra, A. G. Marques, and A. Ribeiro, "Connecting the dots: Identifying network structure via graph signal processing," *IEEE Signal Processing Magazine*, vol. 36, no. 3, pp. 16–43, 2019.
- [61] A. Miraki, H. Saeedi-Sourck, N. Marchetti, and A. Farhang, "Spectral domain spline graph filter bank," *IEEE Signal Processing Letters*, vol. 28, pp. 469–473, 2021.
- [62] R. A. Horn and C. R. Johnson, *Matrix analysis*. Cambridge university press, 2012.
- [63] T. Biyikoglu, J. Leydold, and P. F. Stadler, *Laplacian eigenvectors of graphs: Perron-Frobenius and Faber-Krahn type theorems*. Springer, 2007.
- [64] S. Kurras, U. Luxburg, and G. Blanchard, "The  $f$ -Adjusted Graph Laplacian: a Diagonal Modification with a Geometric Interpretation," in *Proceedings of the 31st International Conference on Machine Learning*, vol. 32, no. 2, Beijing, China, 22–24 Jun 2014, pp. 1530–1538.
- [65] H. E. Egilmez, E. Pavez, and A. Ortega, "Graph learning from data under laplacian and structural constraints," *IEEE Journal of Selected Topics in Signal Processing*, vol. 11, no. 6, pp. 825–841, 2017.
- [66] E. Pavez, B. Girault, A. Ortega, and P. A. Chou, "Region adaptive graph Fourier transform for 3D point clouds," in *2020 IEEE Intl. Conf. on Image Proc. (ICIP)*. IEEE, 2020.
- [67] A. Anis, A. Gadde, and A. Ortega, "Efficient sampling set selection for bandlimited graph signals using graph spectral proxies," *IEEE Transactions on Signal Processing*, vol. 64, no. 14, pp. 3775–3789, 2016.
- [68] F. Dörfler and F. Bullo, "Kron reduction of graphs with applications to electrical networks," *IEEE Transactions on Circuits and Systems I: Regular Papers*, vol. 60, no. 1, pp. 150–163, 2012.
- [69] D. Gleich, "The matlabgl matlab library," 2015.
- [70] B. Girault, S. S. Narayanan, A. Ortega, P. Gonçalves, and E. Fleury, "Grasp: A matlab toolbox for graph signal processing," in *2017 IEEE International Conference on Acoustics, Speech and Signal Processing (ICASSP)*. IEEE, 2017, pp. 6574–6575.
- [71] M. X. Goemans and D. P. Williamson, "Improved approximation algorithms for maximum cut and satisfiability problems using semidefinite programming," *Journal of the ACM (JACM)*, vol. 42, no. 6, pp. 1115–1145, 1995.
- [72] B. Aspöqvist and J. R. Gilbert, "Graph coloring using eigenvalue decomposition," *SIAM Journal on Algebraic Discrete Methods*, vol. 5, no. 4, pp. 526–538, 1984.
- [73] S. Shekizhar and A. Ortega, "Graph construction from data by non-negative kernel regression," in *ICASSP 2020-2020 IEEE International Conference on Acoustics, Speech and Signal Processing (ICASSP)*. IEEE, 2020, pp. 3892–3896.
- [74] Y. Tanaka, Y. C. Eldar, A. Ortega, and G. Cheung, "Sampling signals on graphs: From theory to applications," *IEEE Signal Processing Magazine*, vol. 37, no. 6, pp. 14–30, 2020.



## IX. PROPERTIES AND PROOFS

### A. Proof of Proposition 6

Recall that  $\mathbf{Q}$  from (33) obeys

$$\mathbf{Q} = \mathbf{D}^{bi} + \mathbf{L}^{bd} = \mathbf{D} - \mathbf{W}^{bd}. \quad (79)$$

Using this notation, the fundamental matrix can be written

$$\mathbf{Z} = \mathbf{I} - (\mathbf{D} - \mathbf{W}^{bd})^{-1} \mathbf{W}^{bi}. \quad (80)$$

Because  $\mathbf{Q}^{-1}$  is non negative, and  $\mathbf{Z}\mathbf{1} = \mathbf{0}$ , the matrix  $(\mathbf{D} - \mathbf{W}^{bd})^{-1} \mathbf{W}^{bi}$  is right stochastic. In fact, we can write it as follows

$$(\mathbf{D} - \mathbf{W}^{bd})^{-1} \mathbf{W}^{bi} = \mathbf{Q}^{-1} \mathbf{W}^{bi} = \mathbf{P}^{bd} \mathbf{P}^{bi}, \quad (81)$$

where  $\mathbf{P}^{bi} = (\mathbf{D}^{bi})^{-1} \mathbf{W}^{bi}$ , and  $\mathbf{P}^{bd} = ((\mathbf{D}^{bi})^{-1} (\mathbf{D}^{bi} + \mathbf{L}^{bd}))^{-1}$ , are right stochastic matrices. We can verify this by computing

$$(\mathbf{D}^{bi})^{-1} \mathbf{W}^{bi} \mathbf{1} = (\mathbf{D}^{bi})^{-1} \mathbf{D}^{bi} \mathbf{1} = \mathbf{1}. \quad (82)$$

Note that  $(\mathbf{P}^{bd})^{-1}$  is right stochastic since

$$\begin{aligned} (\mathbf{D}^{bi})^{-1} (\mathbf{D}^{bi} + \mathbf{L}^{bd}) \mathbf{1} &= (\mathbf{D}^{bi})^{-1} (\mathbf{D}^{bi} \mathbf{1} + \mathbf{L}^{bd} \mathbf{1}) \\ &= (\mathbf{D}^{bi})^{-1} (\mathbf{D}^{bi} \mathbf{1}) = \mathbf{1}. \end{aligned}$$

We have proven that  $(\mathbf{P}^{bd})^{-1} \mathbf{1} = \mathbf{1}$ , and conclude by right multiplying by  $\mathbf{P}^{bd}$ .

### B. Proof of Theorem 5 (Perfect Reconstruction GFB)

The projector onto the eigenspace with eigenvalue  $\lambda$  is

$$\mathbf{P}_\lambda = \sum_{i:\lambda_i=\lambda} \mathbf{u}_i \mathbf{u}_i^\top \mathbf{Q}, \quad (83)$$

It is easy to verify that  $\mathbf{P}_\lambda^2 = \mathbf{P}_\lambda$ , and  $\mathbf{P}_\lambda \mathbf{P}_\gamma = \mathbf{0}$  when  $\lambda \neq \gamma$ . Spectral graph filters can be written using the projectors,

$$\mathbf{H}_i = \sum_{\lambda \in \sigma(\mathbf{M}, \mathbf{Q})} h_i(\lambda) \mathbf{P}_\lambda, \quad \mathbf{G}_i = \sum_{\lambda \in \sigma(\mathbf{M}, \mathbf{Q})} g_i(\lambda) \mathbf{P}_\lambda. \quad (84)$$

Then we have that

$$\mathbf{G}_0 \mathbf{H}_0 + \mathbf{G}_1 \mathbf{H}_1 = \sum_{\lambda \in \sigma(\mathbf{M}, \mathbf{Q})} (g_0(\lambda) h_0(\lambda) + g_1(\lambda) h_1(\lambda)) \mathbf{P}_\lambda, \quad (85)$$

$$\mathbf{G}_0 \mathbf{J} \mathbf{H}_0 - \mathbf{G}_1 \mathbf{J} \mathbf{H}_1 = \sum_{\lambda, \gamma \in \sigma(\mathbf{M}, \mathbf{Q})} (g_0(\lambda) h_0(\gamma) - g_1(\lambda) h_1(\gamma)) \mathbf{P}_\lambda \mathbf{J} \mathbf{P}_\gamma. \quad (86)$$

**Theorem 4** implies  $\mathbf{J} \mathbf{P}_\gamma = \mathbf{P}_{2-\gamma} \mathbf{J}$ . Using orthogonality, the only terms that survive are those for which  $\lambda = 2 - \gamma$ , hence

$$\begin{aligned} \mathbf{G}_0 \mathbf{J} \mathbf{H}_0 - \mathbf{G}_1 \mathbf{J} \mathbf{H}_1 &= \\ \sum_{\lambda \in \sigma(\mathbf{M}, \mathbf{Q})} (g_0(\lambda) h_0(2 - \lambda) - g_1(\lambda) h_1(2 - \lambda)) \mathbf{P}_\lambda \mathbf{J}. \end{aligned} \quad (87)$$

The proof follows directly from these identities. Note that if (24) and (25) are true, then  $\mathbf{G}_0 \mathbf{J} \mathbf{H}_0 - \mathbf{G}_1 \mathbf{J} \mathbf{H}_1 = \mathbf{0}$ , and  $\mathbf{G}_0 \mathbf{H}_0 + \mathbf{G}_1 \mathbf{H}_1 = 2 \sum_{\lambda \in \sigma(\mathbf{M}, \mathbf{Q})} \mathbf{P}_\lambda = 2\mathbf{I}$ . For the converse, assume that  $\mathbf{G}_0 \mathbf{H}_0 + \mathbf{G}_1 \mathbf{H}_1 + \mathbf{G}_0 \mathbf{J} \mathbf{H}_0 - \mathbf{G}_1 \mathbf{J} \mathbf{H}_1 = 2\mathbf{I}$ . Now let  $\gamma \in \sigma(\mathbf{M}, \mathbf{Q})$ . Right multiplication by  $\mathbf{P}_\gamma$  implies (24), while right multiplication by  $\mathbf{P}_{2-\gamma}$  leads to (25).

### C. Proof of Theorem 6 (Q-orthogonal GFB)

We need to show that  $\mathbf{T}_a^\top \mathbf{Q} \mathbf{T}_a = \mathbf{Q}$ . We will use the following properties.

- Since  $\mathbf{Q}$  is block diagonal, we have that  $\mathbf{Q} \mathbf{J} = \mathbf{J} \mathbf{Q}$ .
- If  $\mathbf{H}$  is a spectral filter, then  $\mathbf{H}^\top \mathbf{Q} = \mathbf{Q} \mathbf{H}$ . Indeed  $\mathbf{H} = \mathbf{U} h(\mathbf{\Lambda}) \mathbf{U}^\top \mathbf{Q}$ , then

$$\mathbf{H}^\top \mathbf{Q} = \mathbf{Q} \mathbf{U} h(\mathbf{\Lambda}) \mathbf{U}^\top \mathbf{Q} = \mathbf{Q} \mathbf{H}. \quad (88)$$

Since  $\mathbf{I} + \mathbf{J}$  and  $\mathbf{I} - \mathbf{J}$  have disjoint support,

$$\mathbf{T}_a^\top \mathbf{Q} \mathbf{T}_a = \frac{1}{2} \mathbf{H}_0^\top \mathbf{Q} (\mathbf{I} + \mathbf{J}) \mathbf{H}_0 + \frac{1}{2} \mathbf{H}_1^\top \mathbf{Q} (\mathbf{I} - \mathbf{J}) \mathbf{H}_1 \quad (89)$$

$$= \frac{1}{2} \mathbf{Q} \mathbf{H}_0 (\mathbf{I} + \mathbf{J}) \mathbf{H}_0 + \frac{1}{2} \mathbf{Q} \mathbf{H}_1 (\mathbf{I} - \mathbf{J}) \mathbf{H}_1. \quad (90)$$

Using the projectors  $\mathbf{P}_\lambda$ , we can write

$$\begin{aligned} 2 \mathbf{T}_a^\top \mathbf{Q} \mathbf{T}_a &= \sum_{\lambda \in \sigma(\mathbf{M}, \mathbf{Q})} (h_0^2(\lambda) + h_1^2(\lambda)) \mathbf{Q} \mathbf{P}_\lambda + \\ &\quad \sum_{\lambda \in \sigma(\mathbf{M}, \mathbf{Q})} (h_0(\lambda) h_0(2 - \lambda) - h_1(\lambda) h_1(2 - \lambda)) \mathbf{Q} \mathbf{P}_\lambda \mathbf{J}. \end{aligned} \quad (91)$$

If conditions (47) and (48) are true, then  $\mathbf{T}_a^\top \mathbf{Q} \mathbf{T}_a = \mathbf{Q}$ . To show the converse, we use the same strategy used to prove Theorem 5, where we right multiply by  $\mathbf{P}_\gamma$  and  $\mathbf{P}_{2-\gamma}$ .

### D. Proof of Proposition 9

First, observe that (70) and (72) imply that for each resolution  $\ell$ ,  $\mathbb{E}[\mathbf{a}_\ell \mathbf{d}_\ell^\top] = \mathbf{0}$ . Linearity of the expectation implies that any linear transformation of  $\mathbf{a}_\ell$  is also uncorrelated with  $\mathbf{d}_\ell$ , then  $\mathbb{E}[\mathbf{a}_0 \mathbf{d}_\ell^\top] = \mathbf{0}$  and  $\mathbb{E}[\mathbf{d}_\tau \mathbf{d}_\ell^\top] = \mathbf{0}$ , for all  $\ell \geq 0$ , and for all  $\tau \neq \ell$ . Finally, the covariance of the detail coefficients is

$$\mathbb{E}[\mathbf{d}_\ell \mathbf{d}_\ell^\top] = \mathbf{\Sigma}_{\mathcal{B}_\ell \mathcal{B}_\ell} - \mathbf{\Sigma}_{\mathcal{B}_\ell \mathcal{A}_\ell} \mathbf{\Sigma}_{\mathcal{A}_\ell \mathcal{A}_\ell}^{-1} \mathbf{\Sigma}_{\mathcal{A}_\ell \mathcal{B}_\ell} = ((\mathbf{M}_{\ell+1})_{\mathcal{B}_\ell \mathcal{B}_\ell})^{-1}.$$

We conclude by using the spectral folding property and (74), leading to  $(\mathbf{M}_{\ell+1})_{\mathcal{B}_\ell \mathcal{B}_\ell} = (\mathbf{Q}_{\ell+1})_{\mathcal{B}_\ell \mathcal{B}_\ell} = \mathbf{Q}_{1,\ell}$ .

### E. Derivation of (76)

Since  $\mathbf{Q} = \mathbf{V}^{1/2} (\mathbf{I} - \mathbf{V}^{-1/2} \mathbf{W}^{bd} \mathbf{V}^{-1/2}) \mathbf{V}^{1/2} \succ 0$ , we have that  $\mathbf{V}^{-1/2} \mathbf{W}^{bd} \mathbf{V}^{-1/2} \prec 1$ , and  $\rho(\mathcal{A}) = \|\mathbf{V}^{-1/2} \mathbf{W}^{bd} \mathbf{V}^{-1/2}\| < 1$ . Using triangular inequality we have the bound  $\|\mathbf{Q}\| \leq \|\mathbf{V}\| (1 + \rho(\mathcal{A}))$ . The fact that  $\rho(\mathcal{A}) < 1$  also implies that

$$\mathbf{Q}^{-1} = \mathbf{V}^{-1/2} \left( \mathbf{I} - \mathbf{V}^{-1/2} \mathbf{W}^{bd} \mathbf{V}^{-1/2} \right)^{-1} \mathbf{V}^{-1/2}. \quad (92)$$

The norm of  $\mathbf{Q}^{-1}$  can be bounded as  $\|\mathbf{Q}^{-1}\| \leq \|\mathbf{V}^{-1}\| (1 - \rho(\mathcal{A}))^{-1}$ . Combining the upper bounds for  $\|\mathbf{Q}\|$  and  $\|\mathbf{Q}^{-1}\|$  results in the bound for the condition number

$$\kappa(\mathbf{Q}) \leq \kappa(\mathbf{V}) (1 + \rho(\mathcal{A})) / (1 - \rho(\mathcal{A})). \quad (93)$$

## X. MULTI-CHANNEL FILTER BANK

In this section we study properties of tree structured filter banks formed by concatenating two-channel filter banks. For all resolution levels, the graphs, variation operators and sampling sets are given and fixed. An example with  $L = 3$  levels is depicted in Figure 4.

### A. Analysis and synthesis operators

We assume the input signal is at resolution  $L$ , thus  $\mathbf{a}_L = \mathbf{x}$ . The outputs of the low and high pass channels at resolution  $\ell < L$  are called approximation and detail coefficients, and are denoted by  $\mathbf{a}_\ell$ , and  $\mathbf{d}_\ell$ , respectively. The sampling sets obey  $\mathcal{V}_\ell = \mathcal{A}_\ell$ , and for  $\ell < L$ ,  $\mathcal{A}_{\ell+1} = \mathcal{A}_\ell \cup \mathcal{B}_\ell$ . The graph at resolution  $\ell$  is denoted by  $\mathcal{G}_\ell = (\mathcal{V}_\ell, \mathcal{E}_\ell)$ , and has variation operator  $\mathbf{M}_\ell$  with corresponding inner product matrix  $\mathbf{Q}_\ell$ , chosen so that the  $(\mathbf{M}_\ell, \mathbf{Q}_\ell)$ -GFT has the spectral folding property. The analysis equation at resolution  $\ell$  is given by

$$\begin{bmatrix} \mathbf{a}_\ell^\top & \mathbf{d}_\ell^\top \end{bmatrix}^\top = \mathbf{T}_{\alpha,\ell} \mathbf{a}_{\ell+1}. \quad (94)$$

The synthesis operator is  $\mathbf{T}_{s,\ell}$ , and satisfies

$$\mathbf{a}_{\ell+1} = \mathbf{T}_{s,\ell} \begin{bmatrix} \mathbf{a}_\ell^\top & \mathbf{d}_\ell^\top \end{bmatrix}^\top = \Theta_{0,\ell} \mathbf{a}_\ell + \Theta_{1,\ell} \mathbf{d}_\ell, \quad (95)$$

where we have defined the matrices

$$\Theta_{0,\ell} = \mathbf{G}_{0,\ell} \mathbf{S}_{\mathcal{A}_\ell}^\top, \quad \Theta_{1,\ell} = \mathbf{G}_{1,\ell} \mathbf{S}_{\mathcal{B}_\ell}^\top, \quad (96)$$

with dimensions  $|\mathcal{A}_{\ell+1}| \times |\mathcal{A}_\ell|$ , and  $|\mathcal{A}_{\ell+1}| \times |\mathcal{B}_\ell|$ , respectively. After applying (95) recursively we get the synthesis equation

$$\mathbf{x} = \Theta_{0,L-1} \mathbf{a}_{L-1} + \Theta_{1,L-1} \mathbf{d}_{L-1} = \Psi_0 \mathbf{a}_0 + \sum_{k=0}^{L-1} \Phi_k \mathbf{d}_k. \quad (97)$$

The matrices  $\Psi_k$  and  $\Phi_k$  are given by

$$\Psi_k = \Theta_{0,L-1} \Theta_{0,L-2} \cdots \Theta_{0,k}, \quad \Phi_k = \Psi_{k+1} \Theta_{1,k}, \quad (98)$$

for  $k \in [L-1]$ , and  $\Psi_L = \mathbf{I}$ . By collecting the coefficients into a vector  $\mathbf{c} = [\mathbf{a}_0^\top, \mathbf{d}_0^\top, \dots, \mathbf{d}_{L-1}^\top]^\top$ , we can write

$$\mathbf{x} = [\Psi_0 \quad \Phi_0 \quad \cdots \quad \Phi_{L-1}] \mathbf{c} = \mathcal{T}_s \mathbf{c}, \quad (99)$$

where  $\mathcal{T}_s$  and  $\mathcal{T}_a = \mathcal{T}_s^{-1}$  are the synthesis and analysis operators of the tree structured filter bank, respectively.

### B. Frame bounds

Consider a compression application, where  $\mathbf{c}$  and  $\hat{\mathbf{c}}$  are the unquantized and quantized coefficients, respectively. We would like to write the reconstruction error

$$\mathbf{x} - \hat{\mathbf{x}} = \mathcal{T}_s (\mathbf{c} - \hat{\mathbf{c}}) \quad (100)$$

as a function of the quantization error  $\mathbf{c} - \hat{\mathbf{c}}$ . The challenge, is that the operators  $\mathcal{T}_a$  and  $\mathcal{T}_s$  are not orthogonal (under any norm). This is true even if each two channel filter bank at resolution  $\ell$  is  $\mathbf{Q}_\ell$  orthogonal, in fact

$$\|\mathbf{a}_{\ell+1}\|_{\mathbf{Q}_{\ell+1}}^2 = \|\mathbf{a}_\ell\|_{\mathbf{Q}_{0,\ell}}^2 + \|\mathbf{d}_\ell\|_{\mathbf{Q}_{1,\ell}}^2, \quad (101)$$

where we have defined

$$\mathbf{Q}_{0,\ell} = \mathbf{Q}_{\ell+1}(\mathcal{A}_\ell, \mathcal{A}_\ell), \quad \mathbf{Q}_{1,\ell} = \mathbf{Q}_{\ell+1}(\mathcal{B}_\ell, \mathcal{B}_\ell). \quad (102)$$

Note that if we wanted to write  $\|\mathbf{a}_\ell\|_{\mathbf{Q}_{0,\ell}}^2$  as the sum of the energies of  $\mathbf{a}_{\ell-1}$  and  $\mathbf{d}_{\ell-1}$ , in some norm, and apply recursively (101), we would need that

$$\mathbf{Q}_{0,\ell} = \mathbf{Q}_\ell, \quad (103)$$

which is satisfied by the normalized Laplacians of bipartite graphs at all resolution levels (since  $\mathbf{Q}_{0,\ell} = \mathbf{Q}_\ell = \mathbf{I}$ ).

However, (103) does not hold for other variation operators on arbitrary graphs. Fortunately, we can still establish a relation between the norms of the coefficients at different resolutions. We will present a frame bound that relates the norms of  $\mathbf{x}$  and its coefficients  $\mathbf{c}$ , when the two channel filter bank at level  $\ell$  is  $\mathbf{Q}_\ell$  orthogonal. The frame constants depend on the amount by which (103) is violated. First we recall a basic result that relates different vector norms.

**Lemma 1.** [62] *Let  $\mathbf{R}_1$  and  $\mathbf{R}_2$  be positive definite matrices, then*

$$\alpha \|\mathbf{x}\|_{\mathbf{R}_2}^2 \leq \|\mathbf{x}\|_{\mathbf{R}_1}^2 \leq \beta \|\mathbf{x}\|_{\mathbf{R}_2}^2, \quad (104)$$

for any  $\mathbf{x}$ , where

$$\alpha = \inf_{\mathbf{x} \neq 0} \frac{\mathbf{x}^\top \mathbf{R}_1 \mathbf{x}}{\mathbf{x}^\top \mathbf{R}_2 \mathbf{x}}, \quad \beta = \sup_{\mathbf{x} \neq 0} \frac{\mathbf{x}^\top \mathbf{R}_1 \mathbf{x}}{\mathbf{x}^\top \mathbf{R}_2 \mathbf{x}}. \quad (105)$$

Equalities in (104) are attained if and only if  $\mathbf{R}_1 = c\mathbf{R}_2$  for a given constant  $c > 0$ , in which case  $\alpha = \beta = c$ . For each  $\ell \geq 0$ , we define

$$\alpha_\ell = \inf_{\mathbf{x} \neq 0} \frac{\mathbf{x}^\top \mathbf{Q}_{0,\ell} \mathbf{x}}{\mathbf{x}^\top \mathbf{Q}_\ell \mathbf{x}}, \quad \beta_\ell = \sup_{\mathbf{x} \neq 0} \frac{\mathbf{x}^\top \mathbf{Q}_{0,\ell} \mathbf{x}}{\mathbf{x}^\top \mathbf{Q}_\ell \mathbf{x}}. \quad (106)$$

Also, we define,  $A_{L-1} = B_{L-1} = 1$ , and for  $0 \leq \ell < L-1$ ,

$$A_\ell = \prod_{k=\ell+1}^{L-1} \alpha_k, \quad B_\ell = \prod_{k=\ell+1}^{L-1} \beta_k. \quad (107)$$

We also consider the following inner product matrix

$$\mathbf{Q} = \begin{bmatrix} \mathbf{Q}_{0,0} & \mathbf{0} & \cdots & \mathbf{0} \\ \mathbf{0} & \mathbf{Q}_{1,0} & \ddots & \mathbf{0} \\ \vdots & \ddots & \ddots & \vdots \\ \mathbf{0} & \mathbf{0} & \mathbf{0} & \mathbf{Q}_{1,L-1} \end{bmatrix}. \quad (108)$$

Now we present our main result of this section for the tree structured filter bank of Figure 4. The proof is given in Appendix X-C.

**Theorem 7.** *For a  $L$ -level tree structured filter bank, composed of  $\mathbf{Q}_\ell$  orthogonal two channel filter banks, the synthesis operator  $\mathcal{T}_s$  satisfies*

$$C \|\mathbf{c}\|_{\mathbf{Q}}^2 \leq \|\mathcal{T}_s \mathbf{c}\|_{\mathbf{Q}_L}^2 \leq D \|\mathbf{c}\|_{\mathbf{Q}}^2, \quad (109)$$

for all  $\mathbf{x} = \mathcal{T}_s \mathbf{c}$ , with constants given by

$$C = \min_{0 \leq \ell \leq L-1} A_\ell, \quad D = \max_{0 \leq \ell \leq L-1} B_\ell. \quad (110)$$

Now we can revisit (100) and bound the reconstruction error using Theorem 7, leading to  $\|\mathbf{x} - \hat{\mathbf{x}}\|_{\mathbf{Q}_L}^2 \leq D \|\mathbf{c} - \hat{\mathbf{c}}\|_{\mathbf{Q}}^2$ , where  $\mathbf{Q}$  is given by (108).

**Remark 4.** *We have established that the synthesis operator  $\mathcal{T}_s$  is a frame with constants  $C$  and  $D$  [5], [8]. A frame is called tight, if the constants in the upper and lower bound are equal. In this case,  $C = D$  when (103) is true for all  $\ell \geq 0$ . GFBs are tight frames when all the graphs  $\mathcal{G}_\ell$  are bipartite, and BFBs are used for each  $\ell \geq 0$ , since we have that  $A = B = 1$ ,  $\mathbf{Q}_L = \mathbf{Q} = \mathbf{I}$ , and  $\|\mathcal{T}_s \mathbf{c}\|_{\mathbf{I}} = \|\mathbf{c}\|_{\mathbf{I}}$ .*

The constants  $C$ ,  $D$ , and the inner product  $\mathbf{Q}_L$  and  $\mathbf{Q}$  that appear in Theorem 7 depend on the graphs, variation operators and downsampling sets chosen at each resolution level.

C. Proof of [Theorem 7](#) (frame bound of tree structured GFBs)

Let  $\mathbf{c} = [\mathbf{a}_0^\top, \mathbf{d}_0^\top, \dots, \mathbf{d}_{L-1}^\top]$ , and  $\mathbf{x} = \mathcal{T}_s \mathbf{c}$ . The reason we cannot apply [\(101\)](#) recursively, is because [\(103\)](#) does not hold. We can instead use [Lemma 1](#), and the inequalities

$$\alpha_\ell \|\mathbf{a}_\ell\|_{\mathbf{Q}_\ell}^2 \leq \|\mathbf{a}_\ell\|_{\mathbf{Q}_{0,\ell}}^2 \leq \beta_\ell \|\mathbf{a}_\ell\|_{\mathbf{Q}_\ell}^2. \quad (111)$$

Indeed, using  $\mathbf{Q}_L$  orthogonality and [\(111\)](#) implies

$$\|\mathbf{x}\|_{\mathbf{Q}_L}^2 = \|\mathbf{a}_{L-1}\|_{\mathbf{Q}_{0,L-1}}^2 + \|\mathbf{d}_{L-1}\|_{\mathbf{Q}_{0,L-1}}^2 \quad (112)$$

$$\leq \beta_{L-1} \|\mathbf{a}_{L-1}\|_{\mathbf{Q}_{L-1}}^2 + \|\mathbf{d}_{L-1}\|_{\mathbf{Q}_{0,L-1}}^2. \quad (113)$$

We apply  $\mathbf{Q}_\ell$  orthogonality and [\(111\)](#) for each  $\ell \leq L-1$  and,

$$\|\mathbf{x}\|_{\mathbf{Q}_L}^2 \leq B_0 \|\mathbf{a}_0\|_{\mathbf{Q}_{0,0}}^2 + \sum_{\ell=0}^{L-1} B_\ell \|\mathbf{d}_\ell\|_{\mathbf{Q}_{1,\ell}}^2 \leq D \|\mathbf{c}\|_{\mathbf{Q}}^2. \quad (114)$$

We can use the lower bounds in [\(111\)](#), to get the lower bound

$$C \|\mathbf{c}\|_{\mathbf{Q}}^2 \leq A_0 \|\mathbf{a}_0\|_{\mathbf{Q}_{0,0}}^2 + \sum_{\ell=0}^{L-1} A_\ell \|\mathbf{d}_\ell\|_{\mathbf{Q}_{1,\ell}}^2 \leq \|\mathbf{x}\|_{\mathbf{Q}_L}^2. \quad (115)$$